Alma Mater Studiorum - Università di Bologna

SCUOLA DI SCIENZE

Dipartimento di Chimica Industriale "Toso Montanari"

Corso di Laurea Magistrale in

Chimica Industriale

Classe LM-71 - Scienze e Tecnologie della Chimica Industriale

Conformational Analysis and Absolute Configuration of Spiropyrazolones

Tesi di laurea sperimentale

CANDIDATO

Chiara Marchesi

RELATORE

Chiar.mo Prof. Andrea Mazzanti

CORRELATORE

Dr. Michele Mancinelli

Anno Accademico 2016-2017

ABSTRACT

The relative configuration of the four stereocenters of spiropyrazolones **1**, **epi-1** and **2** was determined by NMR-NOE analysis. It turned out that while compound **1** has the 1R*, 2S*, 3R*, 4S* relative configuration, **epi-1** is the diastereoisomer at the C-4 (1R*, 2S*, 3R*, 4R* relative configuration).
A full conformational analysis was performed by Molecular Mechanics (MMFF field) scan of the potential energy surface, and the best conformations were optimized by DFT calculations, including the effect of the solvent in the calculations.

The absolute configuration of the three compounds was then determined by the comparison of the Electronic CD spectra with the simulated spectra obtained by TD-DFT calculations. Four different functionals were used to achieve data redundancy and a more reliable assignment. The 1R, 2S, 3R, 4S absolute configuration was determined for **1**, the 1R, 2S, 3R, 4R for **epi-1** and the 1S, 2R, 3S, 4R for compound **2**.

ABSTRACT

La configurazione relativa dei quattro stereocentri dei composti **1**, **epi-1** e **2** è stata effettuata mediante la analisi degli esperimenti NOE-NMR. È risultato che il composto **1** ha la configurazione relativa 1R*, 2S*, 3R*, 4S*, mentre **epi-1** è il suo epimero in C-4 e ha quindi configurazione relativa 1R*, 2S*, 3R*, 4R*.

La analisi conformazionale completa è stata effettuata tramite Meccanica Molecolare e le conformazioni ottenute sono state quindi ottimizzate mediante calcoli DFT, includendo in questi l'effetto del solvente (acetonitrile).

La configurazione assoluta dei tre composti è stata quindi determinata mediante la comparazione degli spettri ECD ottenuti sperimentalmente con quelli simulati mediante calcoli TD-DFT, effettuati con quattro diversi funzionali per una maggiore affidabilità dei risultati. Le configurazioni assolute determinate sono 1R, 2S, 3R, 4S per il composto **1**, 1R, 2S, 3R, 4R per **epi-1**, 1S, 2R, 3S, 4R per il composto **2**.

INDEX

1 Introduction

1.1 Synergistic catalysis and cascade reactions

Synergistic catalysis is a synthetic strategy that allows to synthetize compounds that cannot be form with a simple catalytic reaction.

In a traditional catalytic pathway, one catalyst reacts with a single substrate to form an activated species, that will react with a second unactivated substrate.

In a synergistic catalysis, instead, two different catalyst react with two different substrates and two different catalytic cycles, to form two different activated species.

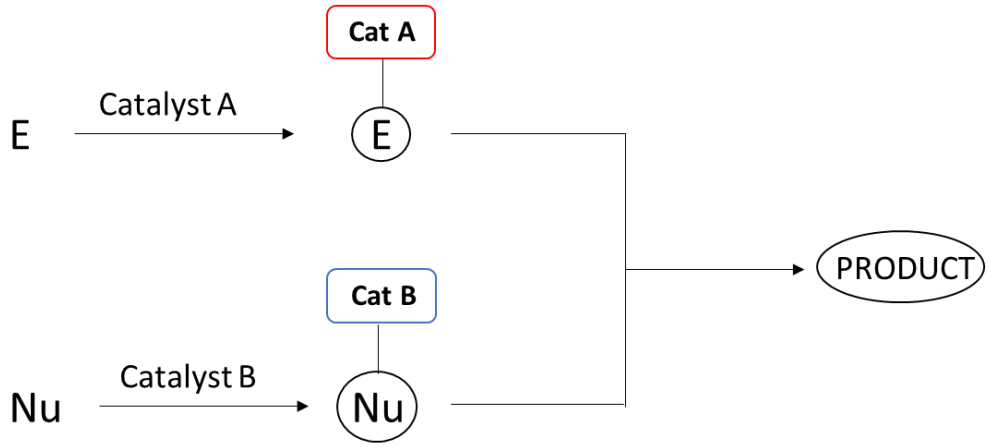

Figure 1 – scheme of the mechanism of the synergistic catalysis.

The so formed activated species has a lower energy of the LUMO orbital and a higher energy of the HOMO orbital, with respect to the ones of the starting materials. The result of this change in the energies of the orbitals is the lowering of the HOMO-LUMO gap and consequently the lowering of the activation energy of the reaction path.

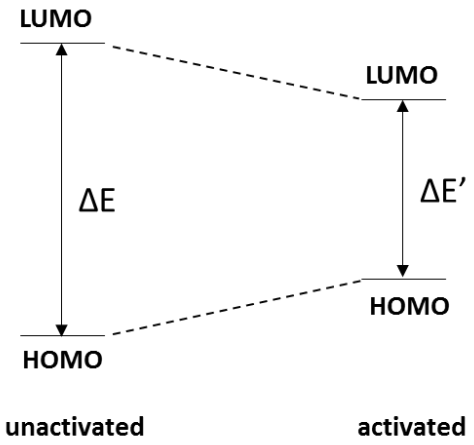

Figure 2 –difference in the HOMO-LUMO energy gap between activated and unactivated species.

The main advantage of this kind of catalysis is, as said before, the possibility to synthetize compounds that cannot be formed with a simple catalytic pathway, but also the possibility to improve the efficiency or the enantioselectivity of existing transformations.

Cascade reactions

A cascade reaction is a chemical process in which consecutive reactions occurs in virtue of the chemical functionality formed in the previous step.[1] Each reaction of the sequence occurs spontaneously, so the isolation of the intermediates is not required.

The earliest example of a cascade reaction is the synthesis of tropinone reported in 1917 by Robinson.[2] Since then, the use of cascade reactions has grown a lot in the area of total synthesis. In contrast to a one-pot procedure, in which occurs consecutive reactions too but is possible to change the reaction conditions or added a new reagent, in a cascade reaction the conditions do not change among the consecutive steps and no new reagents are added after the initial step.[3]

When a cascade reaction takes place intramolecularly it falls under the category of multicomponent reaction.[4] A cascade reaction has a lot of advantages, like the atom economy, the reduction of the waste and the reduction of the times.[5]

Cascades reaction were classified by K. C. Nicolaou in nucleophilic/electrophilic, radical, pericyclic or transition-metal-catalyzed, due to the mechanism of the involved transformations.

The key step of the nucleophilic/electrophilic cascades is a nucleophilic attack. When the attack is driven by an organocatalyst, we are in the case of the organocatalytic cascades, a subcategory of the nucleophilic/electrophilic ones. An example of an organocatalytic cascade reaction is reported in Figure 3:

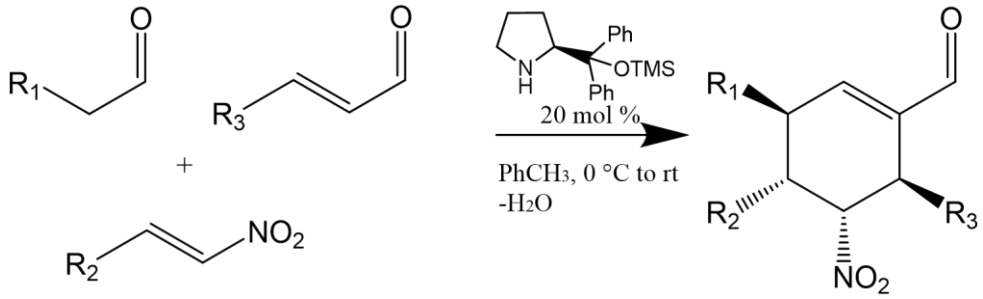

Figure 3 - Asymmetric synthesis of *tetra*-substituted cyclohexane carbaldehydes via a triple organocatalytic cascade reaction.[6]

1.2 Pyrazolone and derivatives

Pyrazolone is a heterocyclic compound derived from pyrazole, that has two possible isomers, shown in Figure 4:

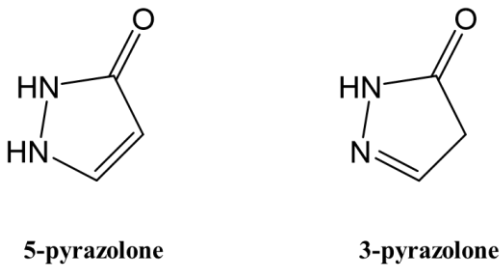

Figure 4 – The two possible isomers of pyrazolone are shown.

Synthesis and chemistry of pyrazolones derivatives have attracted attention due to their many application. In particular, this building block is present in a various kind of drugs: pyrazolone derivatives, for example, act as antimicrobial,[7] analgesic, anti-inflammatory, antipyretic,[8] fungicides,[9] anticancer.[10] Some others have also been shown other properties, like anti-HIV[11] and anti-diabetic.[12]

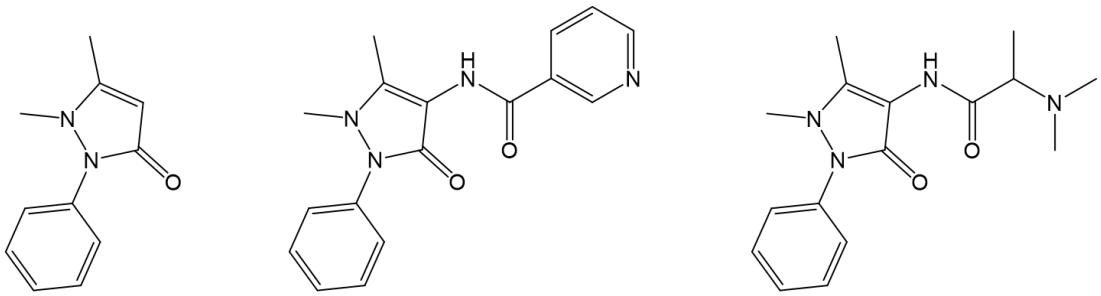

Figure 5 – Some examples of drugs containing pyrazolone scaffold: **a** Fenanzone; **b** Nifenanzone; **c** Aminopropilone.

Due to the several applications of the pyrazolone building block, Rios and coworkers focused their attention on the synthesis of a spiropyrazolone bearing a carbocyclopentane, employing a synergistic cascade reaction. Contrary to carbocyclohexane, carbocyclopentane is difficult to synthetize. Several enantioselective organocatalytic cyclopentanation reactions by Michael addition have been reported,[13] but the limitation is that the synthesis of the starting materials is quite tedious. So, the adopted strategy for the synthesis was the development of a cascade double synergistic catalysis, starting with a bicyclic pyrazolone derivatives and using a transition metal catalyst and amine activation. In particular, a Pd catalyst was used, and to control the the stereoselectivity of the reaction a chiral secondary amine was selected (Figure 6).

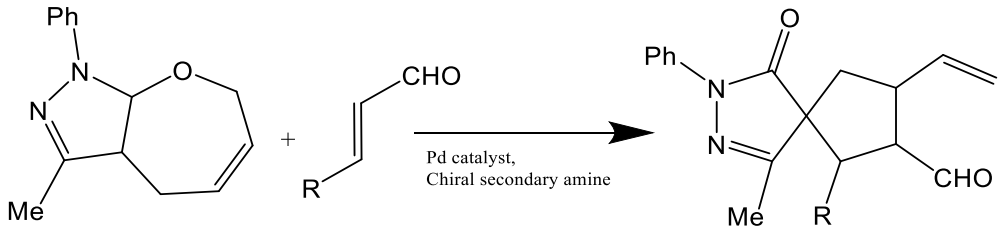

Figure 6 – Synthesis of a generic spiropyrazolone with a double synergistic cascade reaction.

2 Aim of the thesis

As said in section 1, Rios and coworkers focused their attention on the synthesis of spyrazolone derivatives, in particular spiropyrazolones bearing a carbocyclopentane. The adopted strategies for the synthesis were double synergistic cascade reactions, starting from bicyclic pyrazolone derivatives and using Pd and a chiral secondary amine as catalysts. The products of the reaction are spyropyrazolones bearing four new stereocenters, one of which quaternary and spiranic.

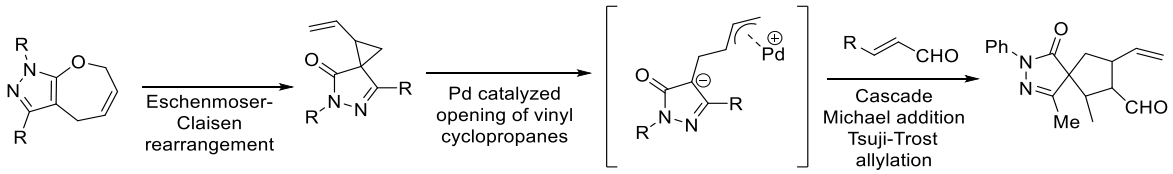

Figure 7 – Preparation of the studied spiropyrazolones.

The determination of the absolute configuration of the chiral carbons is necessary to understand the stereochemical course of the reaction, but it wasn't possible to produce crystals suitable for X-ray analysis, because products are viscous liquid.

The aim of this thesis work was therefore to determine the relative and then the absolute configuration of variously spiropyrazolones using NOE-NMR experiments and chiroptical techniques such as electronic circular dichroism. The studied compounds are shown in Figure **8**:

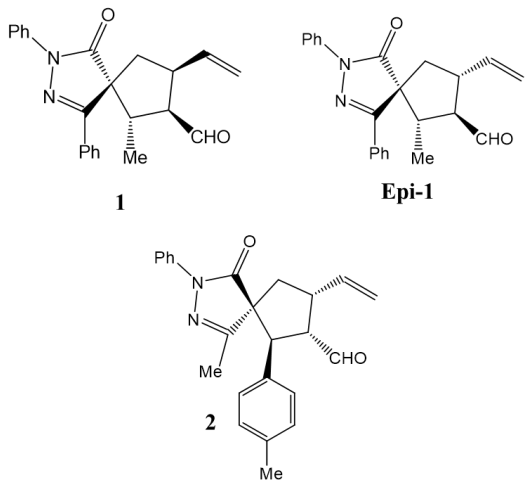

Figure 8 – The studied spiropyrazolones, each with its acronym, are shown.

For each molecule, the investigation was carried out according to a scheme which can be summarized as follows:

1) Assignment of the ^{1}H-NMR chemical shift for each structure.

2) Determination of the relative configuration of the molecules, by means of NOE-NMR experiments.

3) Conformational analysis of the structures determined at the previous point (performed using molecular mechanics) and their subsequent optimizations using DFT calculations.

4) Determination of the absolute configurations by comparison of theoretical simulations of Electronic CD spectra with the experimental one.

3 Results and discussion

3.1 Results for compound 1

Assignment of the ^{1}H-NMR chemical shift

Full assignment of the protons chemical shifts of the molecule was made starting from the signal of the methyl hydrogens, easily identifiable at 0.88 ppm, because it is the only methyl group present in the molecule. Starting from this, it was possible to assign all the aliphatic protons by means of the 2D-COSY experiment (Figure 10). H-2 was identified from the correlation with the methyl hydrogens in the signal at 3.19 ppm. In the same way were determined H-3 at 3.46 ppm (correlation with H-2) and H-4 at 3.92 ppm (correlation with H-3). A fact that confirms the assignment of H-3 is its correlation with the proton of the formyl group at 9.80 ppm (the only aldehydic proton present in the molecule).

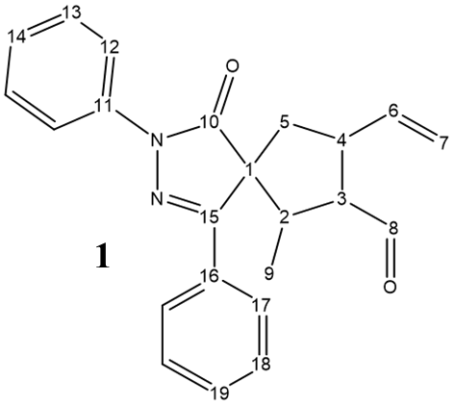

Figure 9 - Compound **1** is shown with carbon number and without protons to clarify.

As well, the identification of the two diastereotopic hydrogens H-5 was made by means of 2D-COSY experiment, that shows the signals of the two hydrogens (from the correlation with the signal of H-4) at 2.33 ppm and at 2.43 ppm. Moreover, from the NOE spectrum (Figure 16) it was possible to discriminate the signal of H-5a from the one of H-5b, obtained from the saturation of the signal of the hydrogen H-4.

From the latter, in fact, was shown the spatial proximity between H-4 and the hydrogen that generate the signal at 2.43 ppm, that is the one in *syn* relationship with respect to it

(named H-5b). Consequently, the signal at 2.33 ppm is the one in the *anti* relationship and named H-5a.

From the COSY correlation with H-4, the vinylic proton H-6 was identified at 5.90 ppm. By exclusion, the signals of the other two vinylic hydrogens (H-7$_E$ and H-7$_Z$) were assigned at 5.12 ppm and 5.23 ppm, respectively. The assignment of the two hydrogens was made by evaluating the typical coupling constants of *trans*-coupling and *cis*-coupling (with respect to H-6); the first one is bigger than the second one, so the signal at 5.23 ppm is that of H-7$_Z$ while the one at 5.12 ppm is that of H-7$_E$.

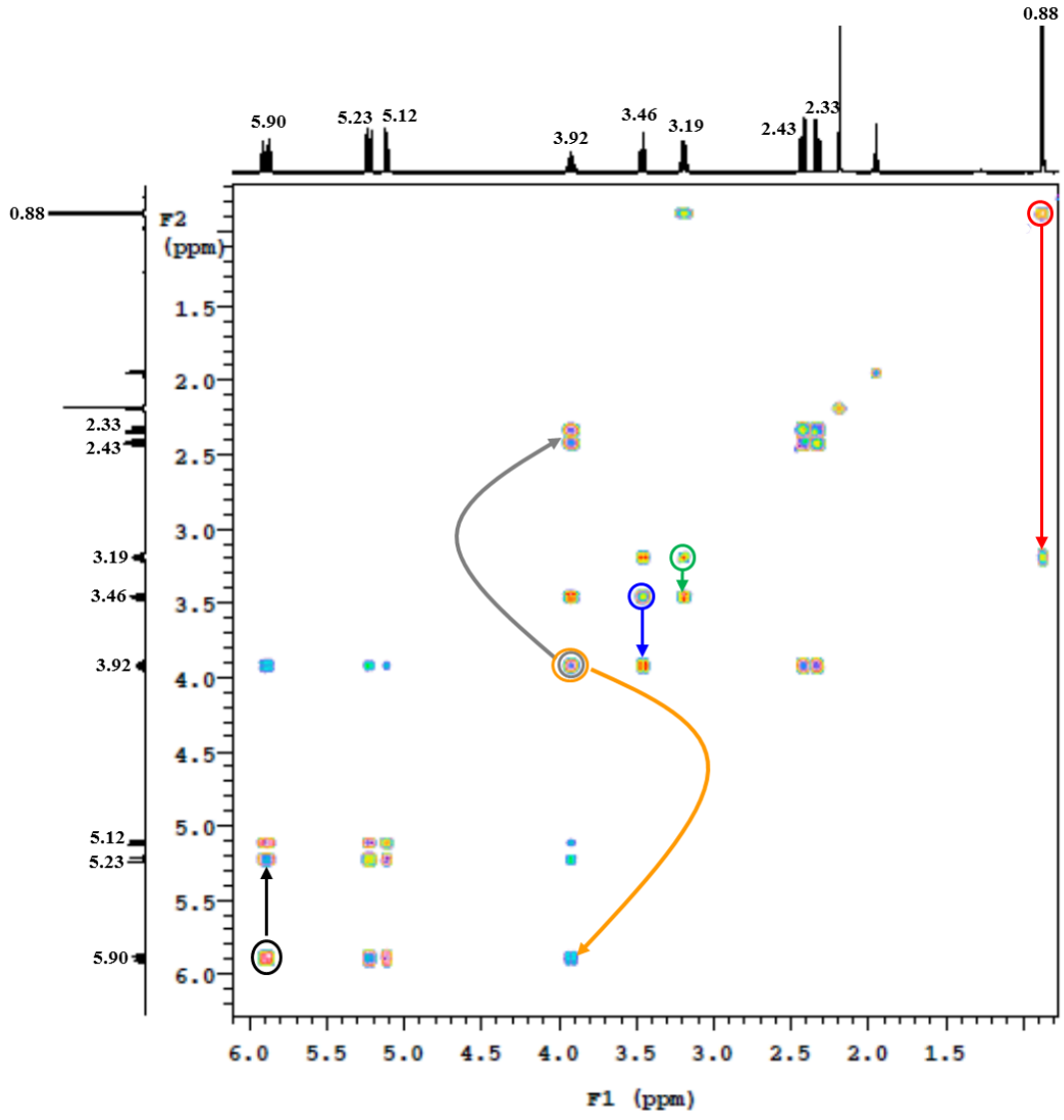

Figure 10 – Aliphatic region of the 2D-COSY spectrum of **1**, used for the assignment of the chemical shift. The coloured arrows represent the correlations between the hydrogen of the molecule. Red: correlation between methyl group and H-2. Green: correlation between H-2 and H-3. Blue: correlation between H-3 and H-4. Grey: correlation between H-4 and the two diastereotopic protons, H-5a and H-5b. Orange: correlation between H-4 and H-6. Black: correlation between H-6 and H-7$_E$/H-7$_Z$

The assignment of the protons of the aromatic region was made starting from the signal at 7.92 ppm, assigned at the hydrogen H-17 on the base of the NOE spectrum obtained from the saturation of H-2 (Figure 11). In this spectrum is shown the spatial proximity of the latter with an *ortho*-aromatic proton, that must be H-17 because of the excessive distance between H-2 and H-12.

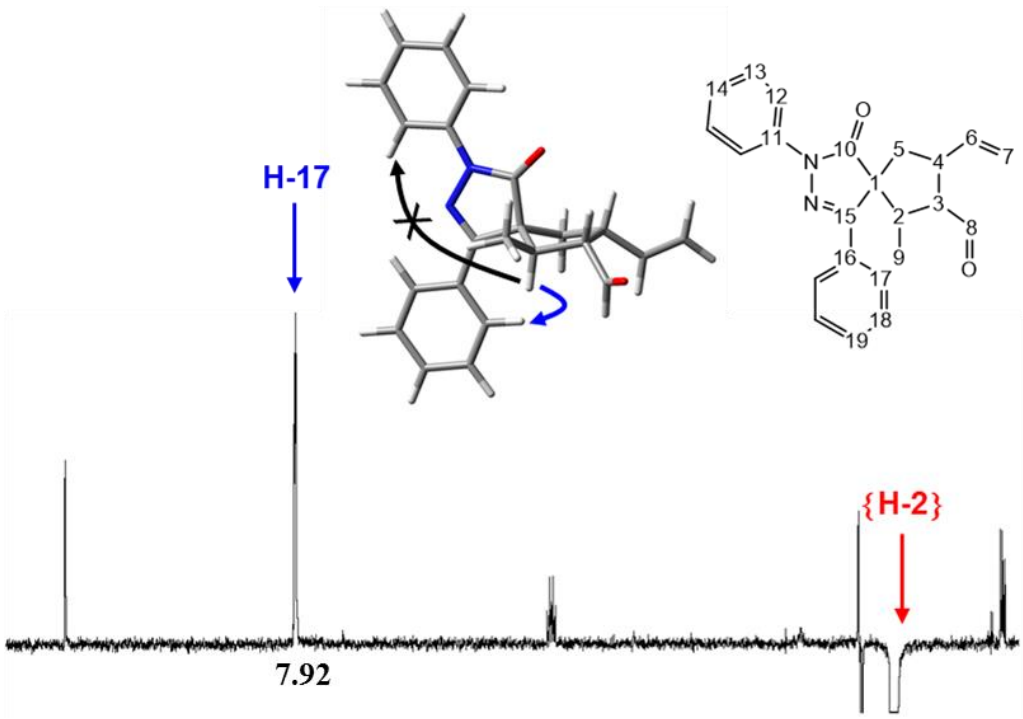

Figure 11– NOE spectrum obtained from the saturation of the hydrogen H-2. In the spectrum is shown the spatial proximity with the *ortho*-aromatic proton H-17 (signal at 7.92 ppm).

H-18 was identified in the signal at 7.54 ppm by means of the 2D-COSY experiment, from its correlation with H-17. In the same way, H-19 was identified in the other signal at 7.54 ppm (superimposed on the previous) from its correlation with H-18. The signal of H-12 was found at 7.97 ppm by exclusion with H-17 from the characteristics coupling constants of an *ortho*-hydrogen. The signal at 7.47 ppm was then assigned at H-13 by the correlation with H-12.

Finally, the hydrogen H-14 at 7.26 ppm was identified by the correlation with H-13.

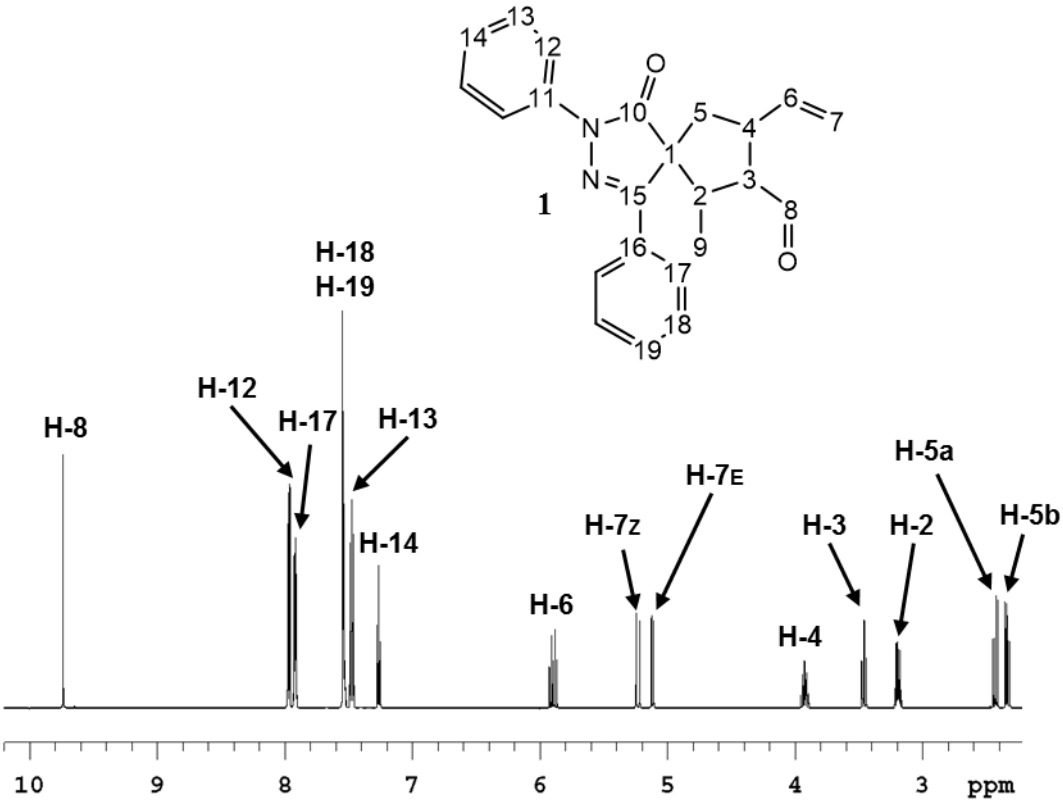

Figure 12- ^{1}H-NMR spectrum of compound **1** is shown with the full assignment of the hydrogens chemical shifts. The signals of H-18 and H-19 are superimposed. The signal of Me-9 is outside the shown spectral region.

Determination of the relative configuration

The determination of the relative configuration of the four stereogenic carbons of the molecule was made by NOE-NMR experiments (Figures 13-18).

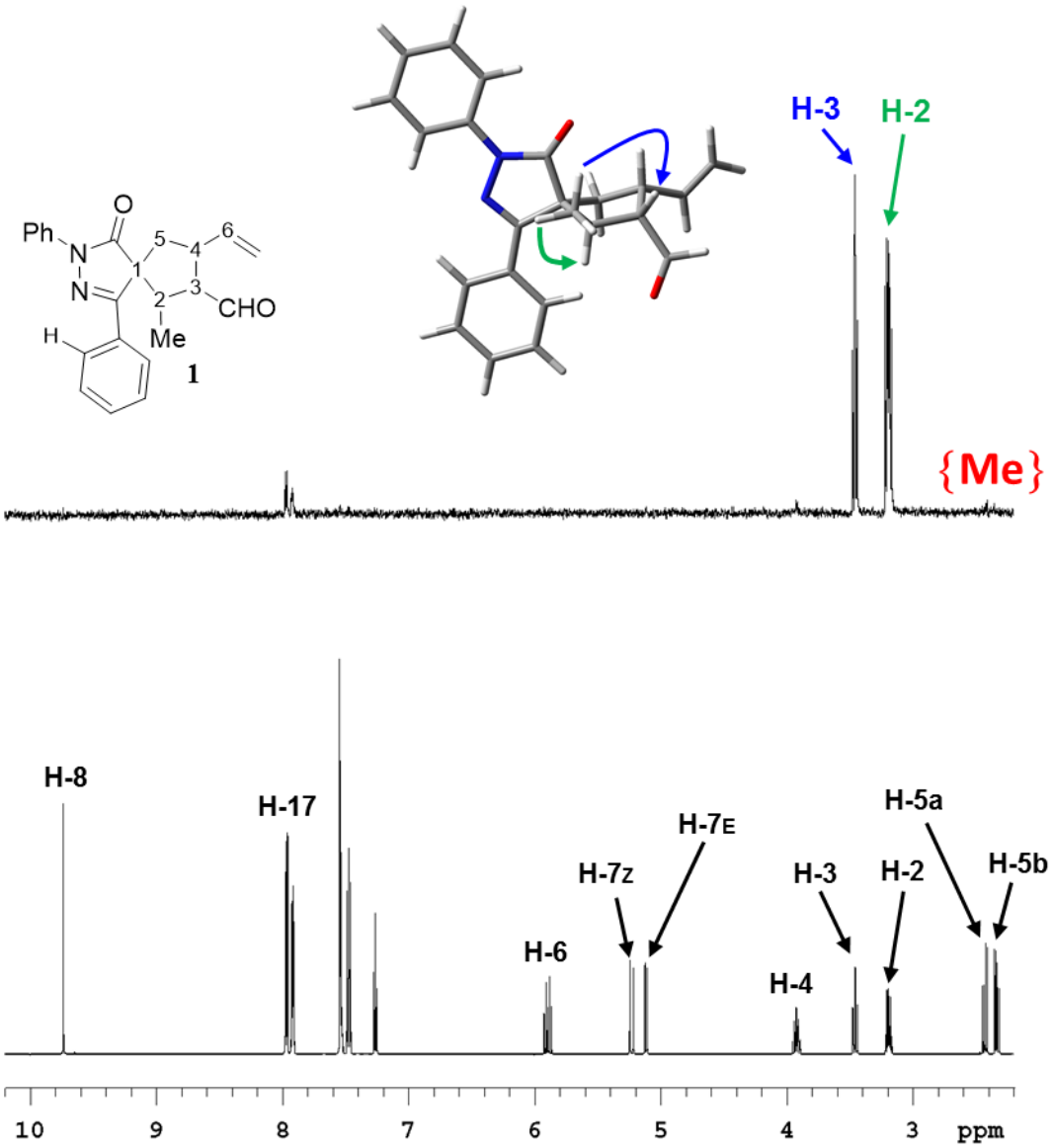

Figure 13 – Top: NOE-NMR spectrum obtained from the saturation of the methyl protons. In green are shown the "control" signals while the blue one reports the relevant information for the determination. Bottom: ^{1}H NMR spectrum.

On saturation of the methyl signal at 0.88 ppm (Figure 13) a strong NOE is observed only on the hydrogen H-3; the NOE effect on H-2, shown in green, is only a "control" NOE that ensures the reliability of the experiment.

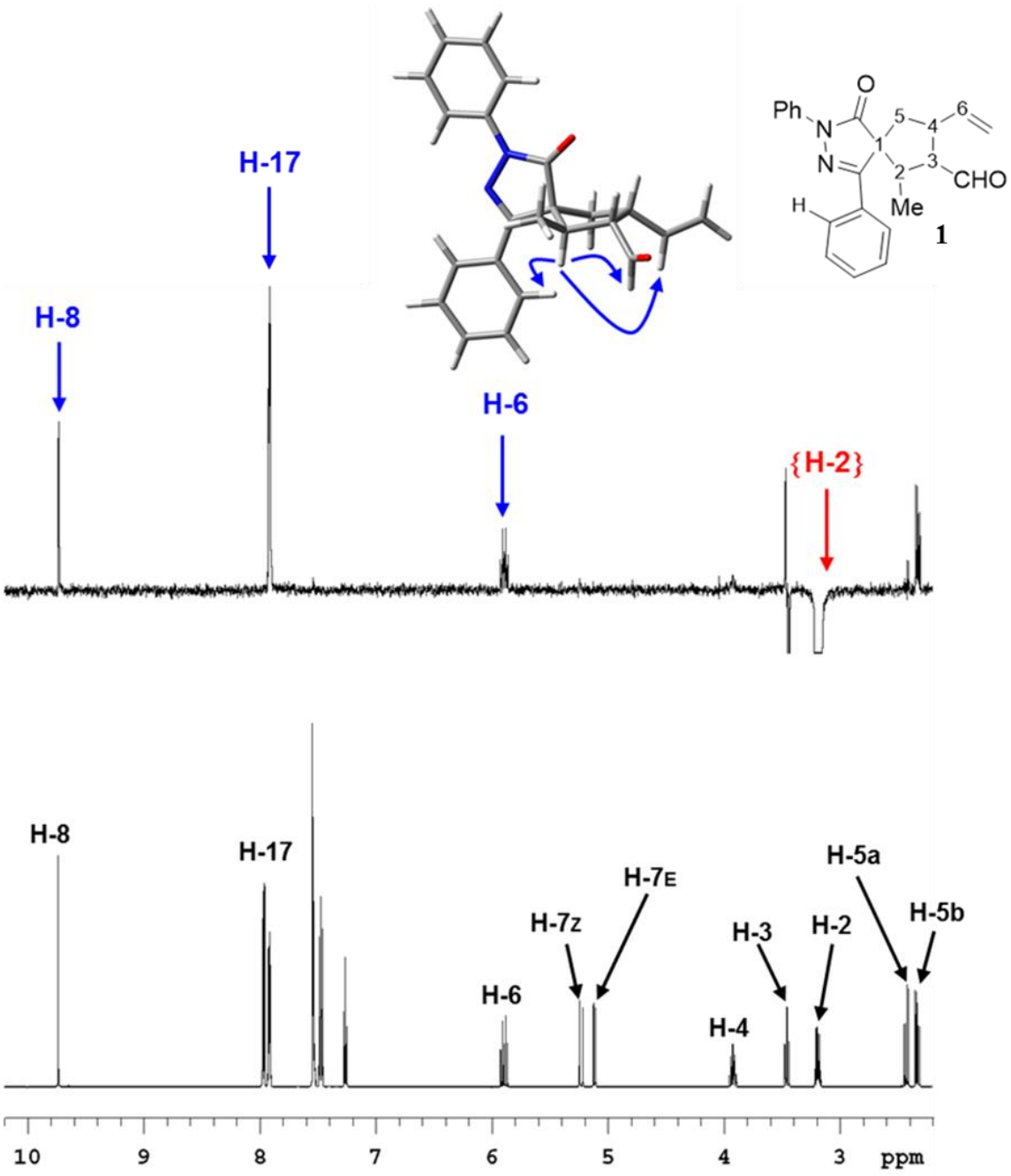

Figure 14 – Top: NOE spectrum obtained from the saturation of H-2. In green are shown the "control" signals while the blue ones report the relevant information for the determination. Bottom: ^{1}H NMR spectrum.

In Figure 14 is shown the NOE spectra obtained from the saturation of H-2. From this, the spatial proximity with H-6, H-17 and H-8 was determined. This spectrum fixes the relative stereochemistry of the two stereogenic carbons C2 and C3.

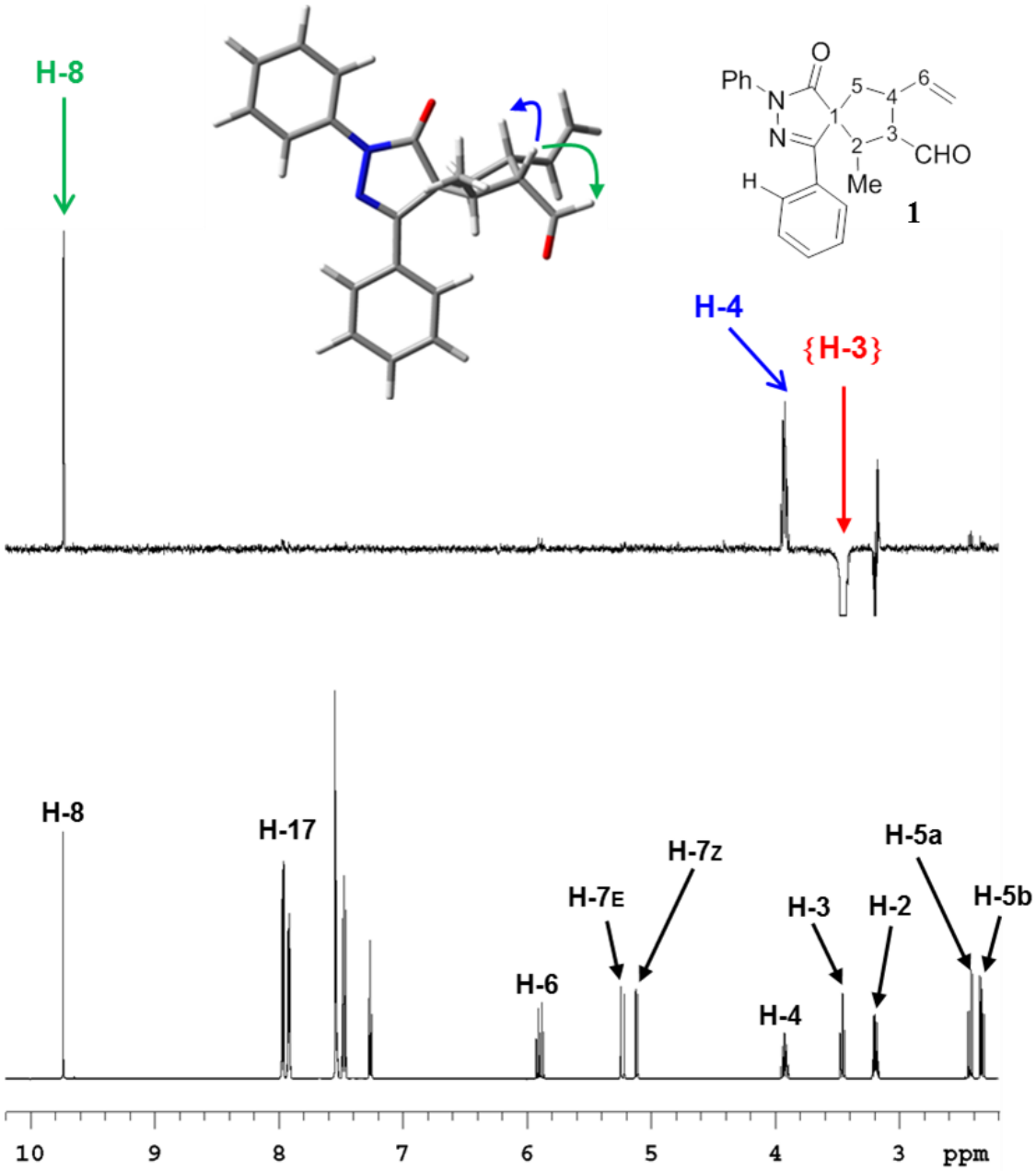

Figure 15 – Top: NOE spectrum obtained from the saturation of the proton H-3. In green are shown the "control" signals while the blue one reports the relevant information for the determination. Bottom: ^{1}H NMR spectrum.

The experiment shown in Figure 15 represent the NOE spectra obtained when the hydrogen H-3 is saturated. With this, it has found its proximity with H-4, while the NOE on H-8 (CHO) is only a control NOE. This spectrum fixes the relative stereochemistry at C4.

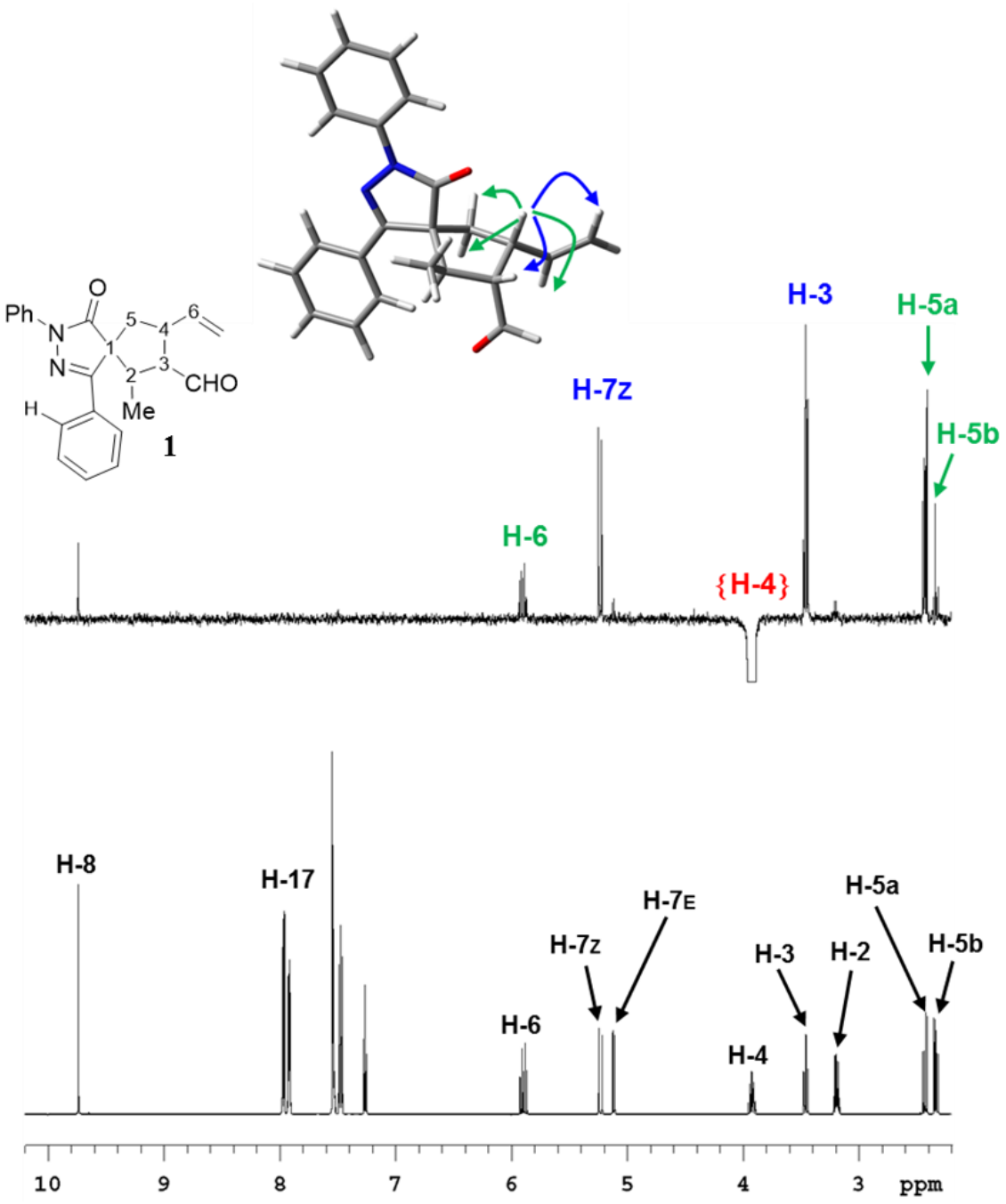

Figure 16 – Top: NOE spectrum obtained from the saturation of H-4. In green are shown the "control" signals while the blue ones report the relevant information for the determination. Bottom: ^{1}H NMR spectrum.

The saturation of H-4 (Figure 16) shows NOE enhancements on H-7z and H-3. The other NOE effects, shown in green, are "control" signals. The strong NOE effect with H-7z (larger than that on H6) suggests a strong conformational preference of the vinyl group, with H-4 and H-6 in *anti* relationship (dihedral angle close to 180°).

The information collected up to now may be enough for the determination of the relative configuration of the molecule, but further NOE spectra were acquired to gain more redundancy and more information about the preferred conformation (Figures 17 and 18).

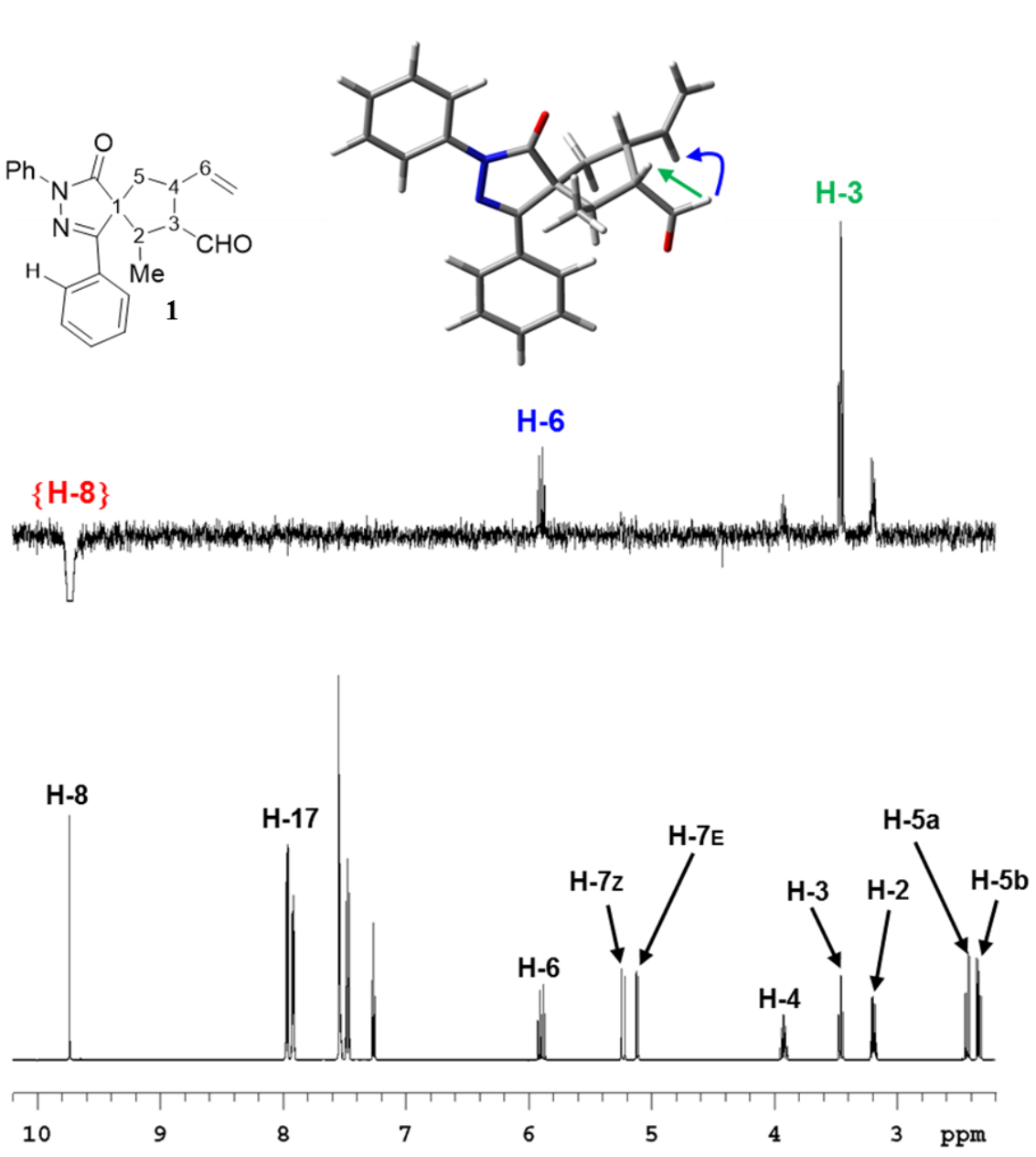

Figure 17 – Top: NOE spectrum obtained from the saturation of H-8. In green are shown the "control" signals while the blue one report the relevant information for the determination. Bottom: ^{1}H NMR spectrum.

In Figure 17, that shows the NOE spectra obtained when H-8 is saturated, the enhancements with H-3 is a control signal, while the important information obtained is the spatial closeness between H-8 and the hydrogen H-6.

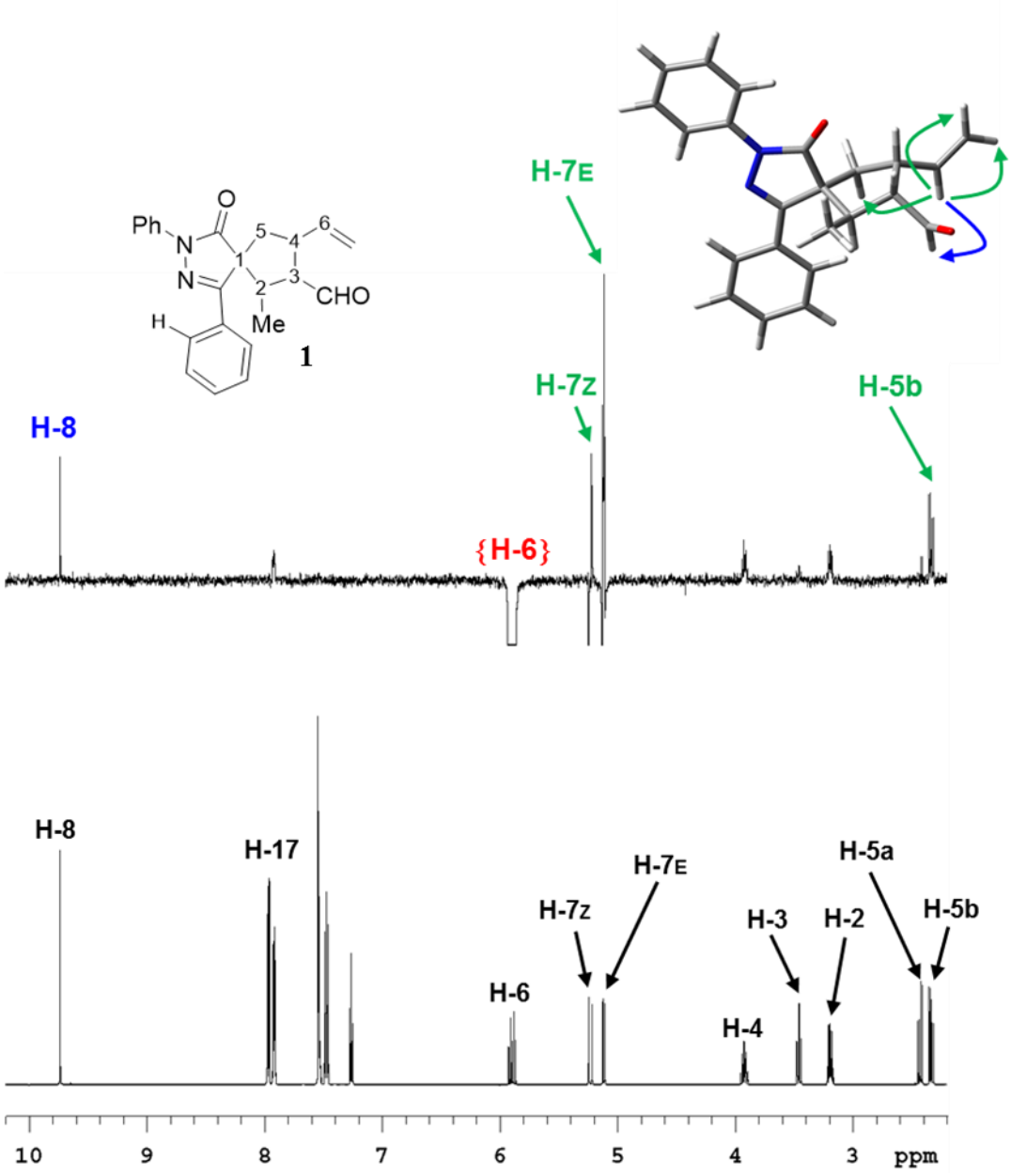

Figure 18 - Top: NOE spectrum obtained from the saturation of the proton H-6. In green are shown the "control" signals while the blue one reports the relevant information for the determination. Bottom: ^{1}H NMR spectrum.

In Figure 18 is shown the NOE spectra obtained when H-6 is saturated. In this is confirmed how already seen in Figure 17, that is the closeness between H-6 and H-8.

With the information collected from the above mentioned spectra, it has been possible to assign the relative configuration of the compound **1**. From the saturation of the signal of the methyl group at 0.88 ppm (Figure 13), a strong NOE effect is observed with H-3, while only tiny enhancements are observable on aromatic hydrogens. This suggest that H-3 and the methyl group are on the same side, and far from the aromatic ring. This

suggestion is confirmed when H-2 is saturated (Figure 14): in this spectrum is visible the closeness between H-2 and H-17, as well as the one with the proton H-8 of the formyl group and with the proton H-6 of the vinyl one. This means that the proton H-2 is near the aromatic ring and on the same side of H-6 and H-8. The strong NOE effect with H-4 obtained when H-3 is saturated suggest that these protons are on the same side of the five-membered ring, and this is confirmed when H-4 is saturated. The last two NOE spectra further confirm what previously seen. From the saturation of H-8 (Figure 17 is clearly visible its closeness with H-6 and *vice versa* for the saturation of H-6 (Figure 18).

The relative configuration obtained for compound **1** is therefore *1R*,2S*,3R*,4S** (assuming to be *R** the configuration of the quaternary spiro carbon).

Conformational analysis

Starting from the assigned relative configuration, a complete conformational analysis was performed in order to find all the low-energy conformations. In the present case, the spiranic structure is rather rigid, but it maintains some degree of conformational freedom. All-carbon five-membered ring can assume different conformations due to its out-of-plane conformation, and the CHO and vinyl moieties can take different orientations.

A full scan of the potential energy surface (PES) was performed using molecular mechanics and the MMFF force field. All the energy minima enclosed in the lowest 10 kcal/mol range were then fully optimized using DFT calculations at the B3LYP/6-31G(d) level of theory. Frequency analysis was performed to check whether they corresponded to ground state (GS)(no imaginary frequencies observed). After DFT optimization, four conformations were found to be enclosed in a ≈ 3 kcal/mol range (Figure 19 and Table 1). They are different, as mentioned for the different relative dispositions of the CHO, vinyl and pyrazolone, with small modification of the ring conformation. In particular, conformation GS3 was obtained from GS1 by rotation of the aldehydic group, while GS2 and GS4 was obtained by rotation of the vinyl group from GS1 and GS3 respectively.

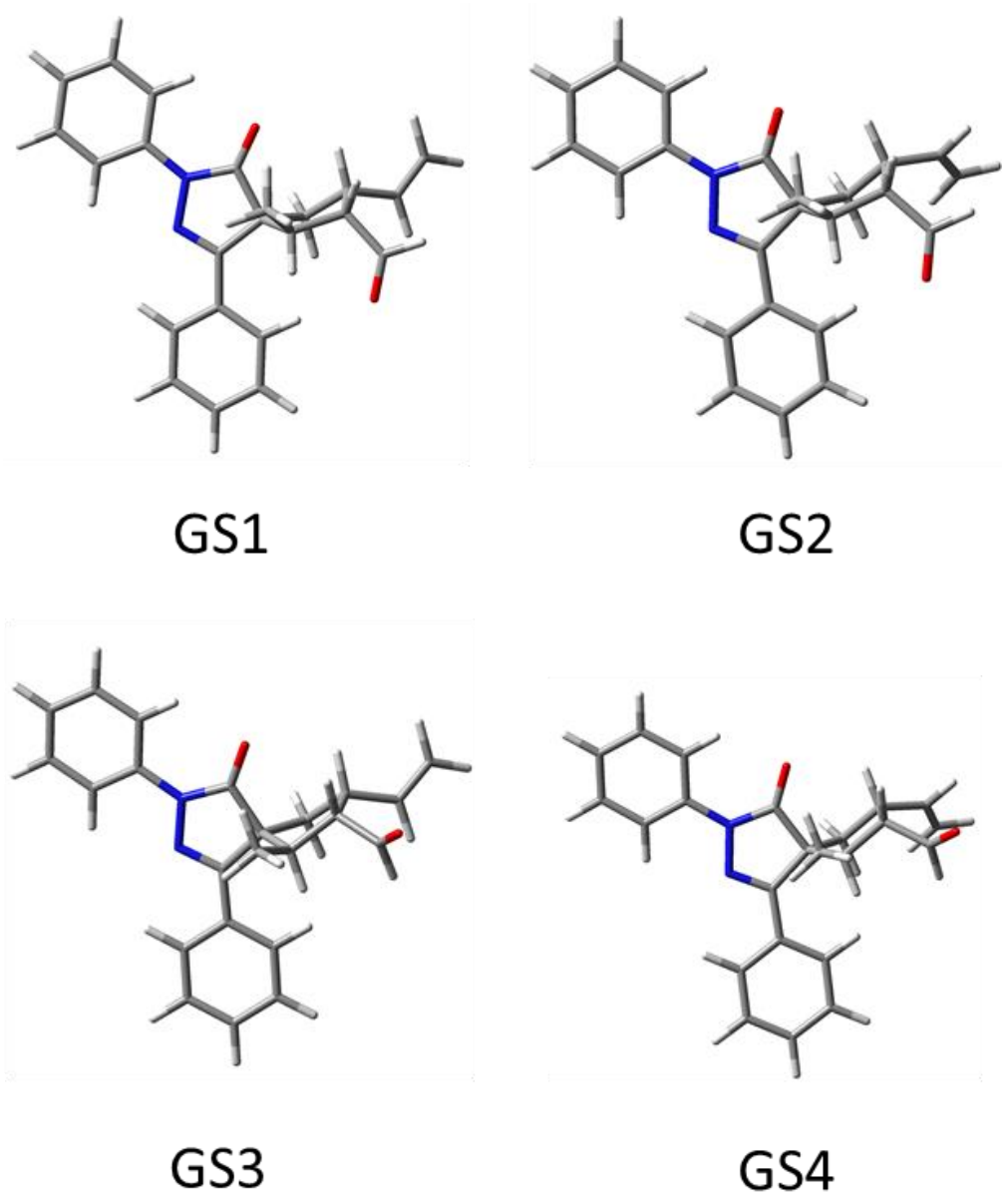

Figure 19 - The four best conformations of **1** optimized at the B3LYP/6-31G(d) level.

Almost all the experimental NOEs well agree with the lowest energy conformation GS1. However, the NOE observed on H-6 when saturating H-2 (Figure 14) suggest that the population of GS3 is not negligible, while calculations suggest a small population (less than 1% at +25 °C, Table 1). DFT calculations were then run again at the B3LYP/6-31G(d) level taking into consideration the solvent (acetonitrile), using the PCM formalism. The new results confirm that GS1 is again the best conformation, but they suggest a larger stabilization of GS3 (10% population) and GS4, in better agreement with

the experimental NOE data, in particular with the NOE observed on H-6 when saturating H-2.

Table 1. Relative energies of the four conformations of **1**, calculated at the B3LYP/6-31G(d) level of theory (energies in kcal/mol).

Conf.	Gas phase			PCM (acetonitrile)		
	E	H°	Pop(H)	E	H°	Pop(H)
GS1	0.00	**0.00**	84.4	0.00	**0.00**	71
GS2	1.03	1.00	14.8	0.78	0.80	19
GS3	3.10	2.89	0.4	1.44	1.32	8
GS4	3.40	3.12	0.3	2.91	2.04	2

Determination of the absolute configuration

The reference method to assign the absolute configuration relies on the X-ray anomalous scattering.[14] This approach requires the preparation of enantiopure single crystals, and the presence of a suitable heavy atom in the molecule (Z>Si when using Mo-Kα radiation).[15]

In the present case, these requirements are not fulfilled and compound **1** is a viscous liquid. So, the anomalous dispersion X-ray crystallography is unfeasible. For this reason, the absolute configuration was determined by the theoretical simulations of chiro-optical spectra. The determination of the absolute configuration (AC) of chiral molecules using chiroptical techniques such as optical rotation (OR) and circular dichroism (Electronic CD and Vibrational CD) has become very reliability because of the development of theoretical methods for the prediction of these properties based on DFT (for VCD) and on Time-Dependent DFT (for ECD).[16]

In the case in question, the theoretical calculation of ECD spectra was selected for the absolute configuration assignment of **1**. The ECD spectrum of **1** was acquired in HPLC-grade acetonitrile solution (about $1 \cdot 10^{-4}$ M) with a cell path of 0.2 cm in the 190-400 nm

region by the sum of 16 scans at 50 nm/min scan rate (figure 20). Albeit rather weak, the experimental ECD spectrum exhibits a broad positive Cotton effect centred at 305 nm and 255 nm and two negative branches at 275 nm and 233 nm. The most intense region of the spectrum has a positive band at 215 nm and a negative one at 195 nm.

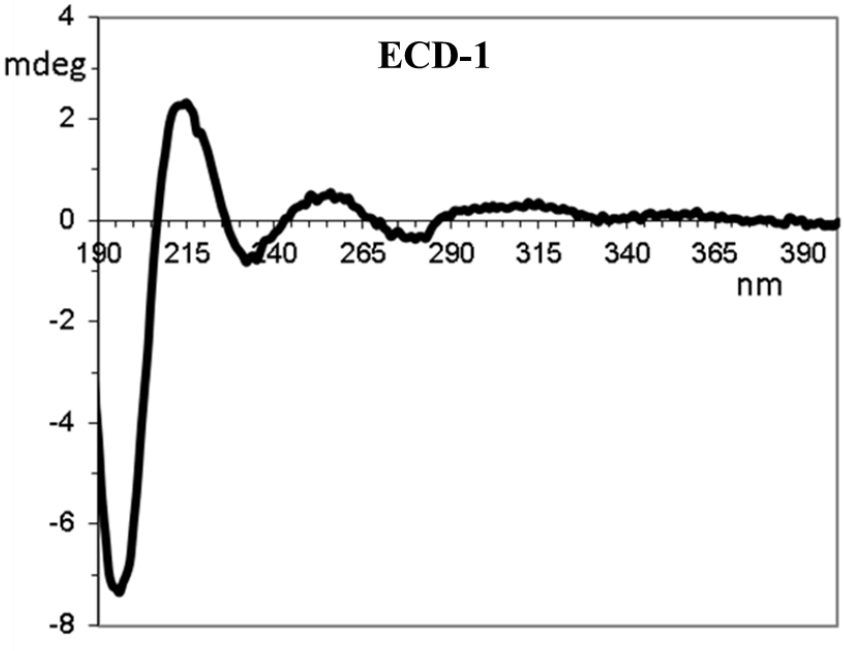

Figure 20 – Experimental ECD spectrum of **1** in acetonitrile.

The TD-DFT simulations of the ECD spectra were performed using the geometries of the four conformations GS1-GS4 optimized at the PCM-B3LYP/6-31G(d) level. For data redundancy and to get more reliability, calculations were performed with the hybrid functionals BH&HLYP[17] and M06-2X,[18] with ωB97XD that includes empirical dispersion,[19] and with CAM-B3LYP[20] that includes long range correction using the Coulomb Attenuating Method. The calculations included the contribution of the solvent using the PCM formalism, and employed the 6-311++G(2d,p) basis set, that is known to yield good performances at a reasonable computational cost.[21] The rotational strengths were calculated in both length and velocity representation, obtaining similar results (RMS difference < 5%) that ruled out large basis set incompleteness errors (BSSE).[22] The results of the TD-DFT calculations, assuming the 1*S*,2*R*,3*S*,4*R* absolute configuration are shown in Figure 21.

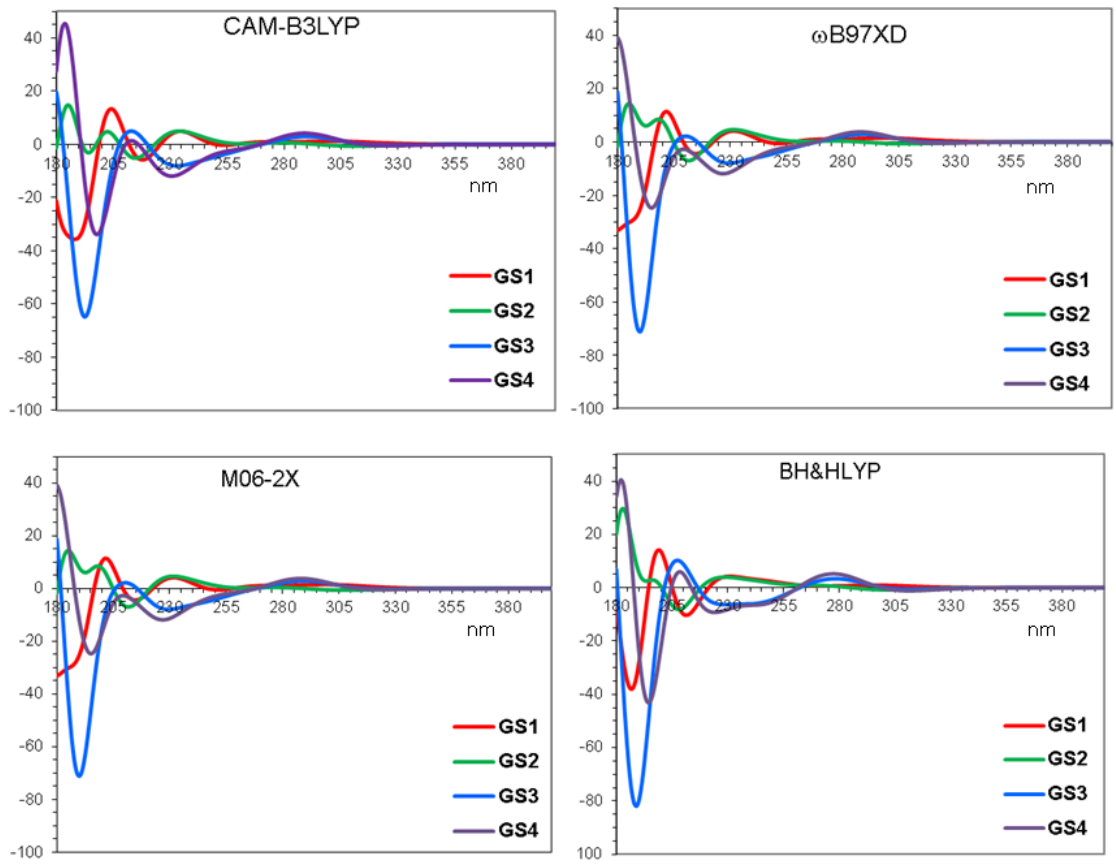

Figure 21 - TD-DFT simulated spectra calculated for the four conformations of **1** using CAM-B3LYP, BH&HLYP, M06-2X, ωB97XD and the 6-311++G(2d,p) basis set. Solvent acetonitrile was included with the PCM formalism. For each conformation, the first 70 excited states were calculated, and the spectrum was obtained using a 0.25 eV line width at half height.

All the simulations suggest a broad positive band at about 290 nm, while the band at 235 nm has different sign for different conformations, being positive in GS1 and GS2 and negative for GS3 and GS4. The two pairs of conformations are different because of the conformation of the formyl moiety. The higher energy region is mainly negative in conformation GS1, GS2 and GS4, while GS3 is weaker and positive. To obtain the calculated spectrum to be compared with the experimental one, the four simulated spectra were weighted using the populations obtained from Boltzmann distribution, and considering the relative energies obtained with the PCM-optimization (Table 1, 71:19:8:2 ratio).

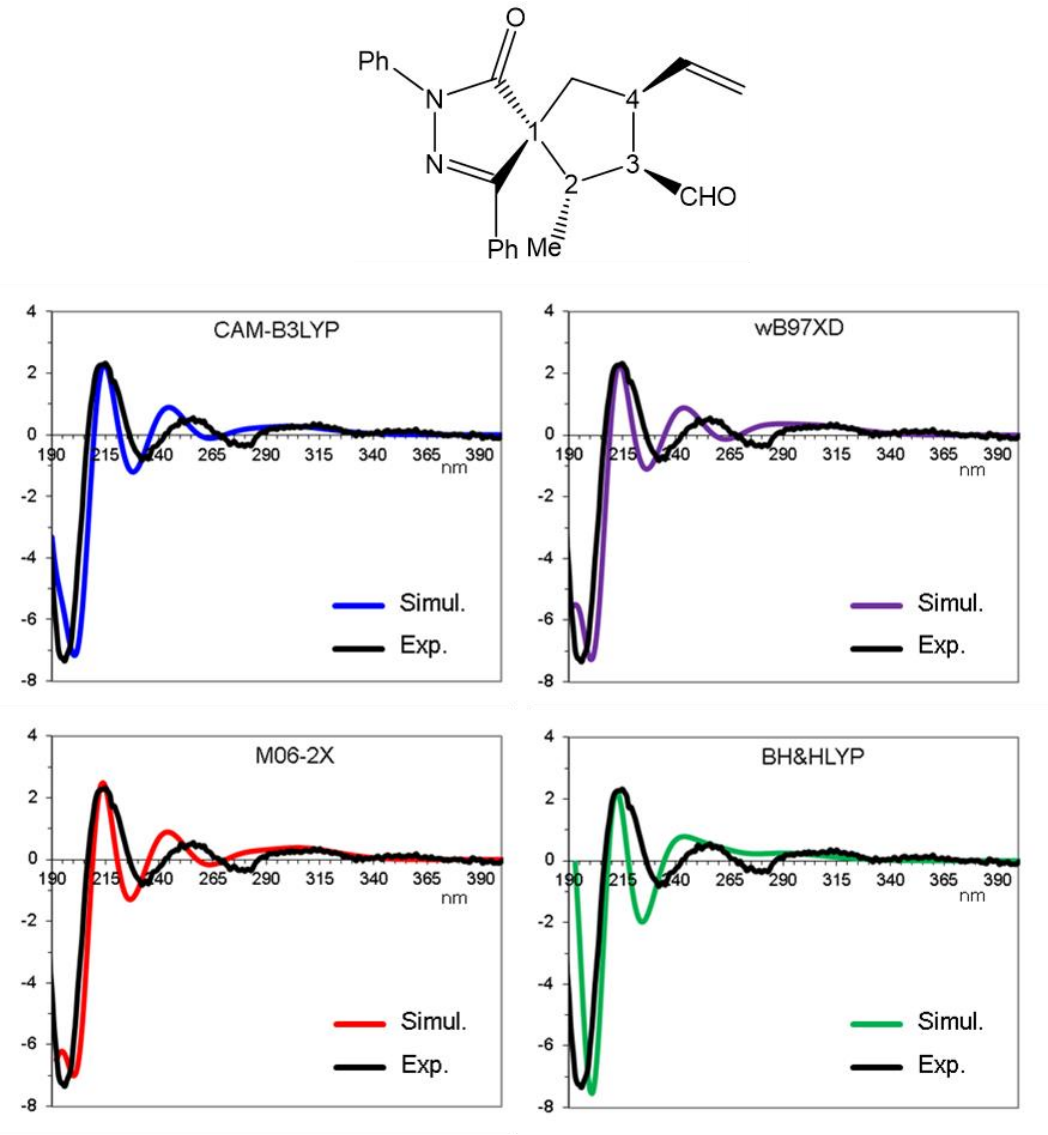

Figure 22- Simulations of the experimental ECD spectrum of **1**. For each quadrant, the black line corresponds to the experimental spectrum. The colored lines correspond to the simulations obtained using the populations derived from PCM-B3LYP/6-31G(d) optimization. All the simulations are for the 1*R*,2*S*,3*R*,4*S* absolute configuration.

The simulated spectra were vertically scaled and red-shifted to get the best match with the experimental spectrum (scaling factors: 0.25, 0.3, 0.3, 0.25; red shift: 10, 12, 12, 13 nm for CAM-B3LYP, ωB97XD, M06-2X and BH&HLYP, respectively). The red-shift was calibrated to match the most intense band at 195 nm. Regarding the shape, the four simulations are in a good agreement with the experimental spectrum. All of them correctly match the sign and sequence of the Cotton effects, but the low energy bands are slightly overestimated in energy (i.e. they are simulated at shorter wavelengths). In any case, the simulation reliably assign the 1*R*,2*S*,3*R*,4*S* absolute configuration.

3.2 Results for compound epi-1

The full NMR assignment of compound **epi-1** has been made in the same way of that already seen for the major diastereoisomers **1**. From the 2D-COSY experiment and starting from the signal of the methyl group at 0.87 ppm, it was possible to identify the hydrogen H-2 at 2.96 ppm (from the correlation with the methyl signal), H-3 at 3.06 ppm (correlation with H-2 and the proton of the formyl group at 9.65 ppm) and H-4 at 3.44 ppm (correlation with H-3). The two diastereotopic protons H-5 were also identified with the 2D-COSY experiment, from the correlation with H-4. From the NOE spectra, it was possible to assign the signal at 2.88 ppm at H-5b (in *syn* relationship with H-4) and the signal at 2.15 ppm at H-5a (in *anti*-relationship with H-4). The vinyl protons were assigned as already seen for the major diastereoisomers **1**: H-6 at 5.98 ppm (from the correlation with H-4), H-7z at 5.22 ppm (from the correlation with H-6 and from the characteristics coupling constant of vinyl hydrogens). In the same way, H-7E at 5.12 ppm (from the correlation with H-6 and from the characteristics coupling constant).

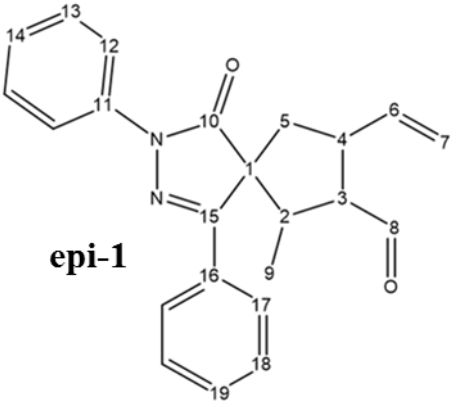

Figure 23 - Compound epi-**1** is shown with carbon number and without proton to clarify.

From the NOE spectrum obtained from the saturation of the hydrogen H-2, it was noted its spatial proximity with the aromatic proton that enhances the signal at 7.98 ppm, corresponding to H-17. At this chemical shift there is the superimposition of two different signals, that of H-17 and that of H-12. From the 2D-COSY experiment, therefore, it was not possible to distinguish with certainty the signal of H-18 from that of H-13 (the two hydrogens that correlate with H-17 and H-12, respectively). The assignment has been made, therefore, by analogy with the case of the major diastereoisomers **1**, because we do not expect a large variation of the chemical shift of

these protons with respect to the previous case. On that basis, the signal at 7.54 ppm was assigned to H-18, and from the 2D-COSY experiment it was possible to see the correlation of this one with the other signal H-19 at 7.54 ppm. For exclusion, the signals of H-13 and H-14 are at 7.48 ppm and 7.26 ppm, respectively.

Relative configuration

Similarly to **1**, the relative configuration of **epi-1** was determined by means of NOE-NMR experiments.

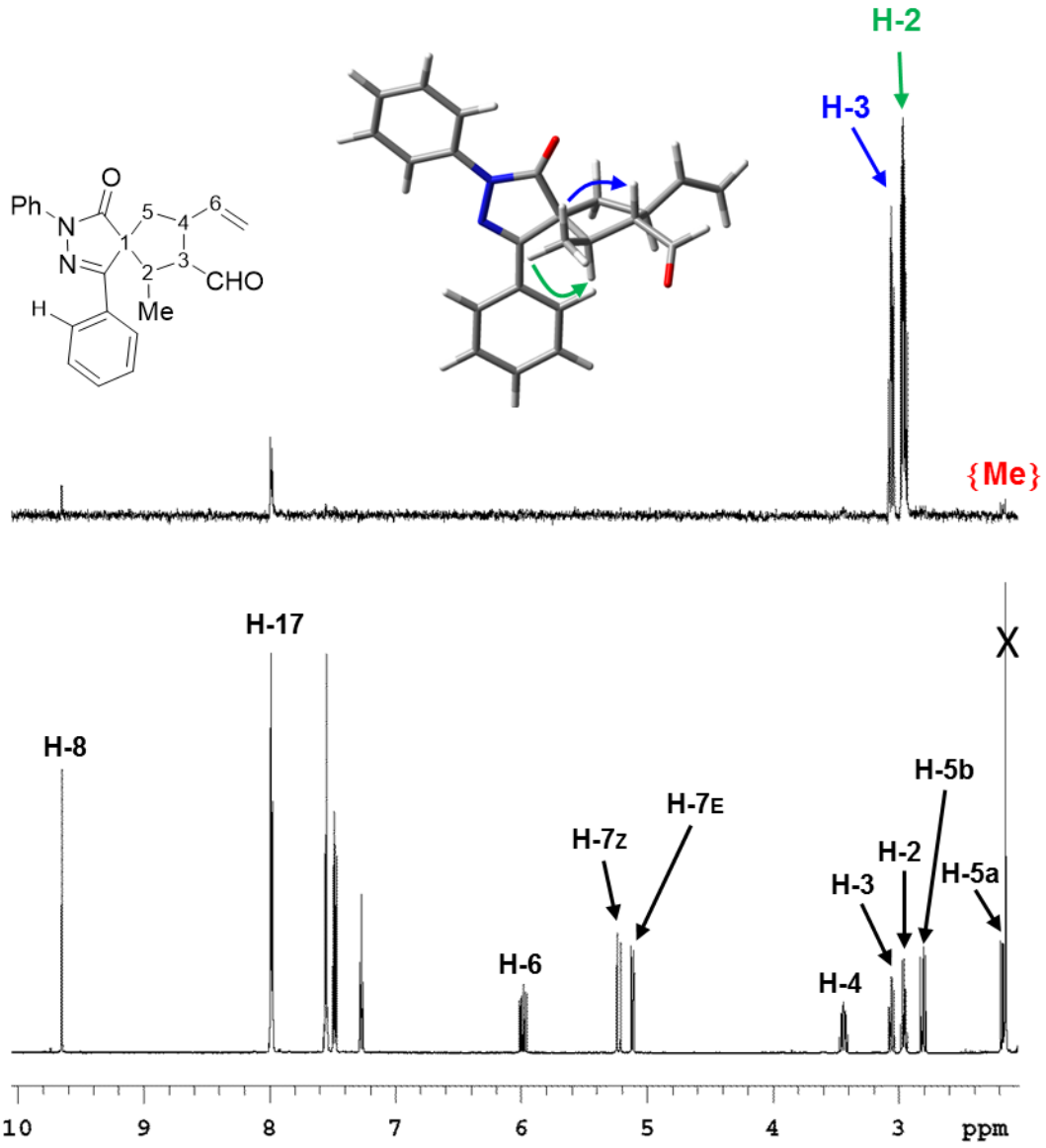

Figure 24 – Top: NOE spectrum obtained from the saturation of the methyl signal. In green are shown the "control" signals while the blue one reports the relevant information for the determination. Bottom: ^{1}H NMR spectrum.

The first experiment, shown in Figure 24, reports the saturation of the methyl signal. The spectra are almost identical to that already seen for the major diastereoisomers **1**. There is a strong NOE effect with H-3 while the NOE with the aromatic hydrogen H-17 is negligible, and also NOE on H-4 is not visible.

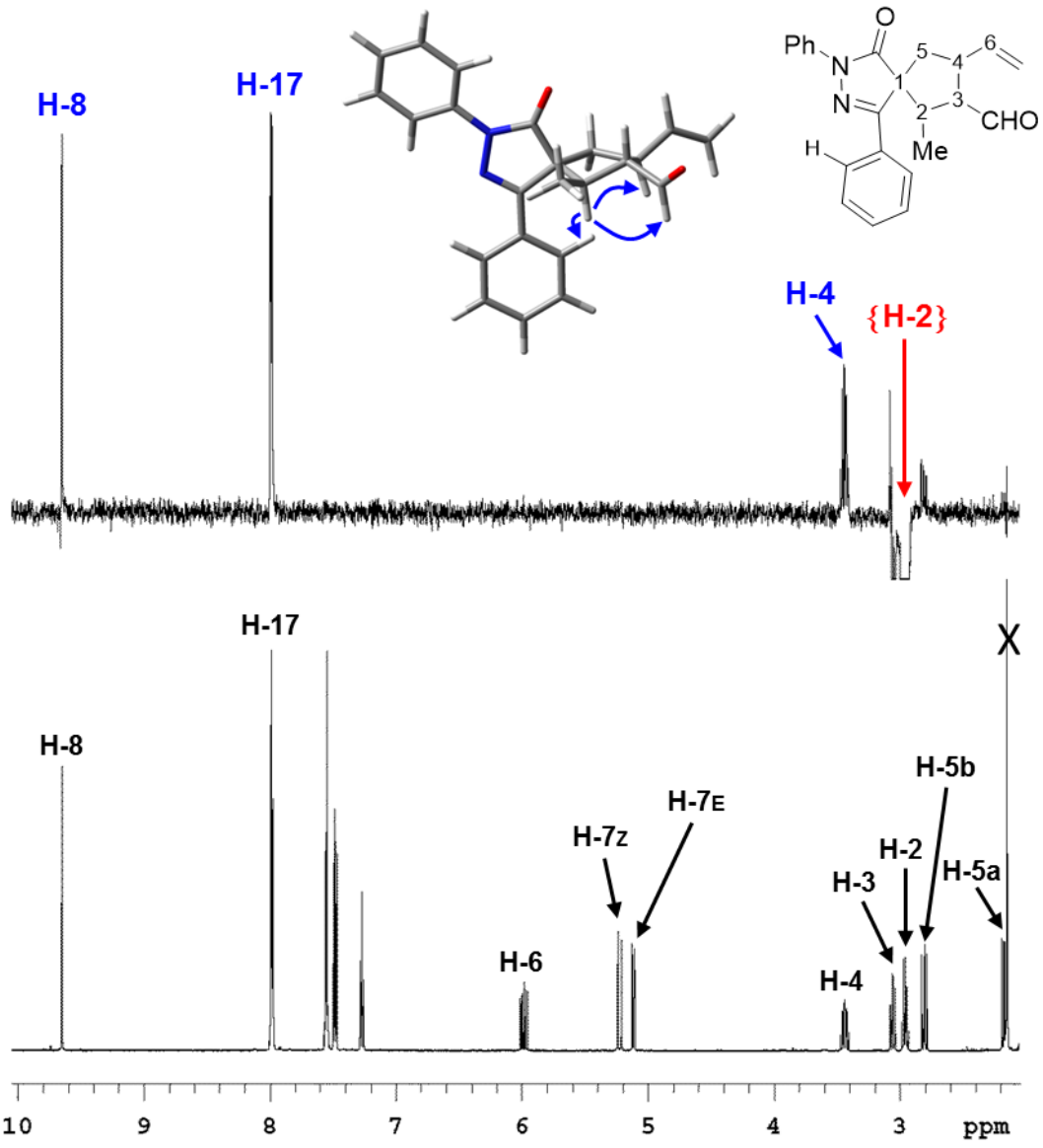

Figure 25 – Top: NOE spectrum obtained from the saturation of the proton H-2. In green are shown the "control" signals while the blue ones report the relevant information for the determination. Bottom: ^{1}H NMR spectrum.

When the signal of H-2 is irradiated, the spectrum shows quite different results from the one of **1**. While in the previous case there was a strong NOE effect on H-6 (as well as

with H-17 and H-8), in this case this NOE effect is not visible, instead a strong NOE is observed on H-4.

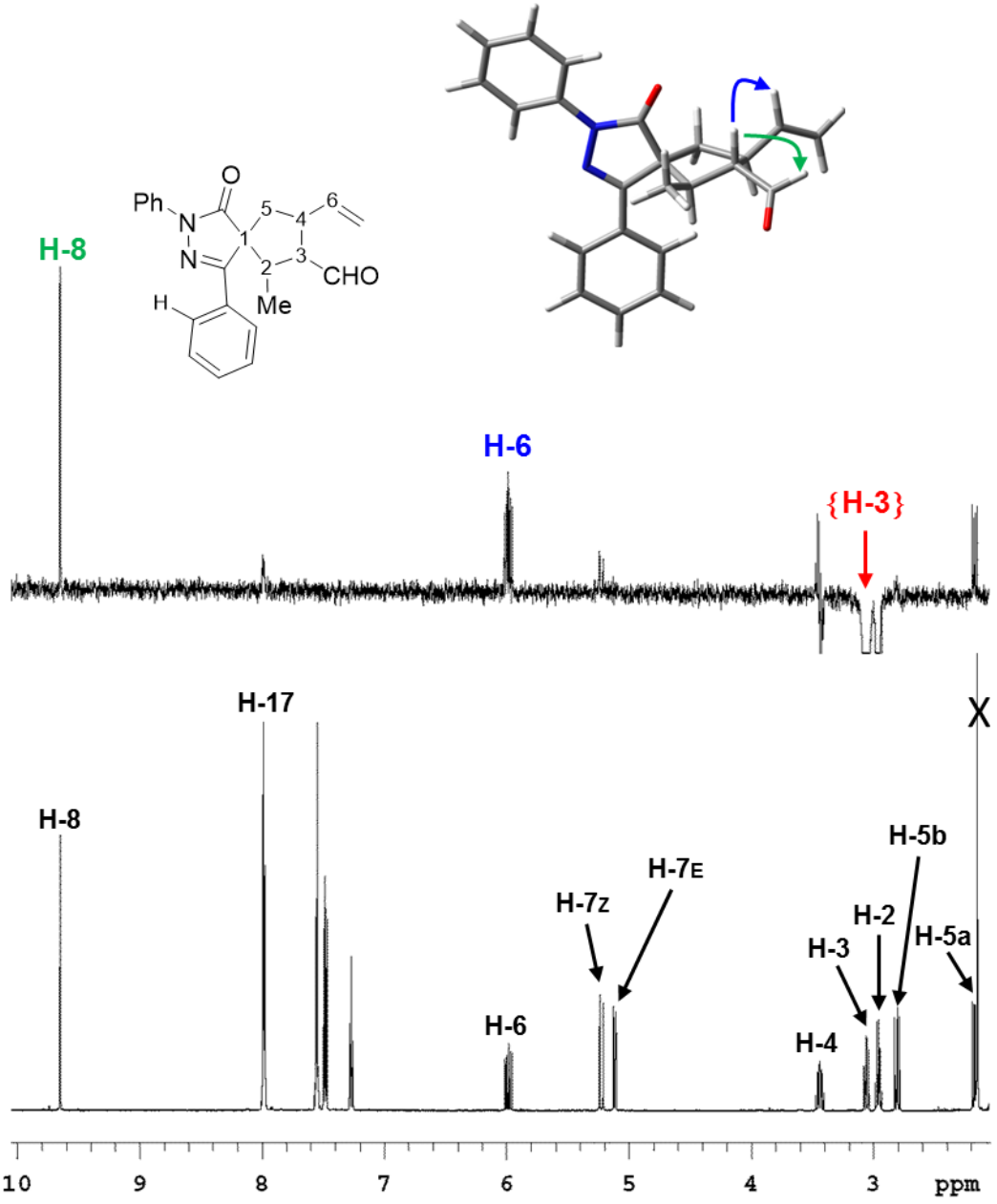

Figure 26 – Top: NOE spectrum obtained from the saturation of the proton H-3. In green are shown the "control" signals while the blue one reports the relevant information for the determination. Bottom: ^{1}H NMR spectrum.

From the saturation of H-3 it was possible to determine the spatial proximity with H-6 and no more with the H-4, as well as in compound **1**. In this spectrum, the NOE effect on H-8 act as a control signal.

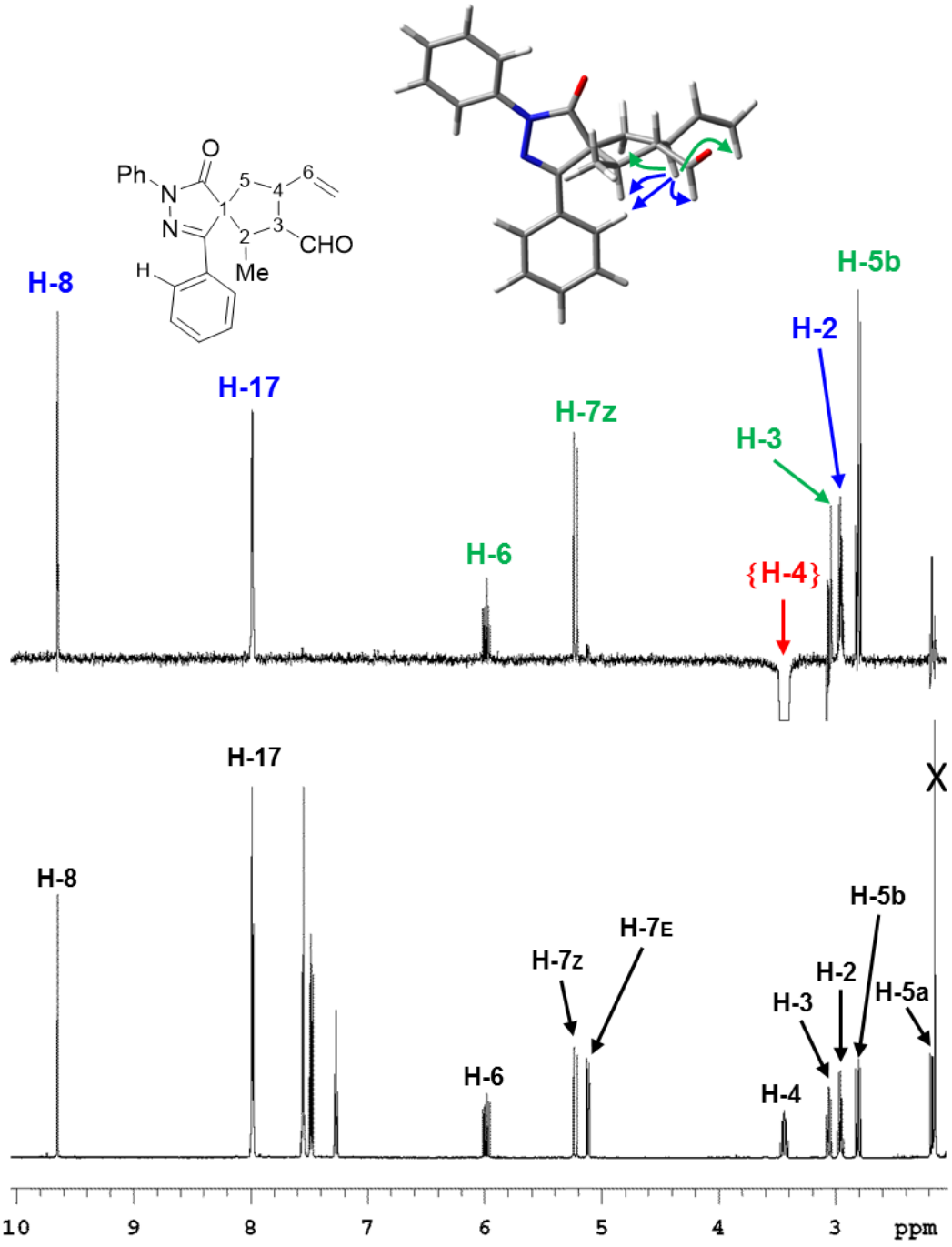

Figure 27 – Top: NOE spectrum obtained from the saturation of the proton H-3. In green are shown the "control" signals while the blue ones report the relevant information for the determination. Bottom: ^{1}H NMR spectrum.

In Figure 27 is shown the spectrum obtained from the saturation of H-4. There are three relevant NOE effects, i.e those with H-2, H-17 e H-8, in contrast to what was seen for compound **1**, where there was a strong NOE with H-3 instead of H-8. In this case it is the opposite. This and the two previous spectra suggest that H-4 and H-3 are on opposite

sides. Also in this case, two more spectra where acquired to get more redundancy of the results.

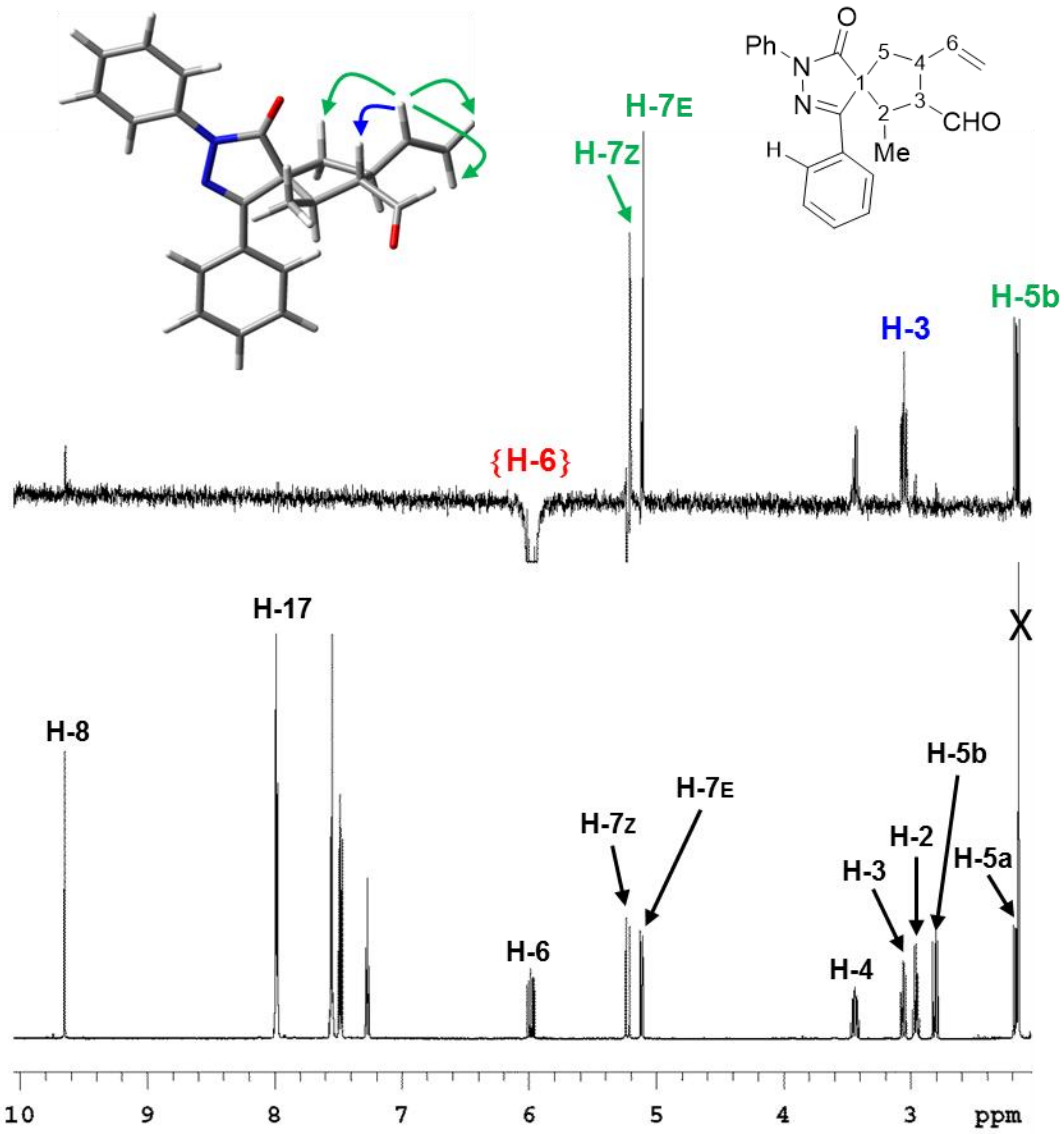

Figure 28 – Top: NOE spectrum obtained from the saturation of H-6. In green are shown the "control" signals while the blue one reports the relevant information for the determination. Bottom: ^{1}H NMR spectrum.

In Figure 28 is confirmed what already seen in Figure 26, i.e. the proximity between H-6 and H-3, in addition to that with vinyl hydrogen H-7E and H-7Z that act as the "control" signals.

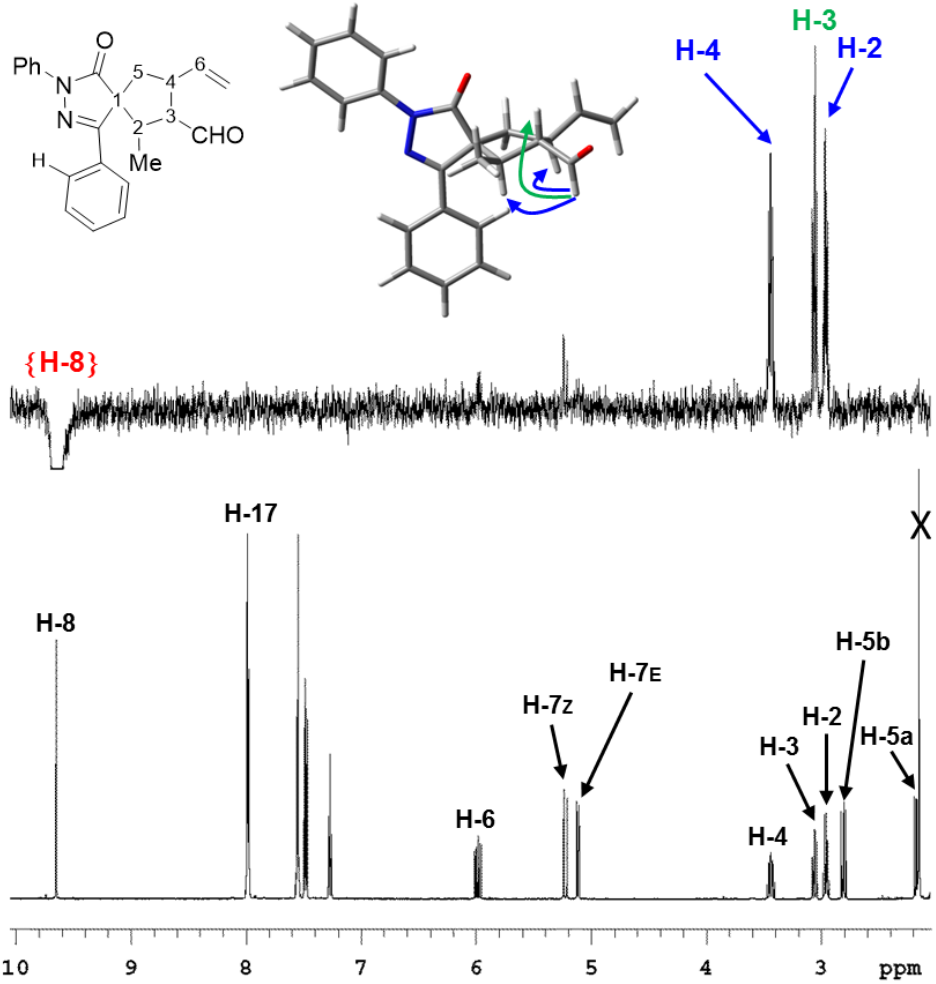

Figure 29 – Top: NOE spectrum obtained from the saturation of H-8. In green are shown the "control" signals while the blue one report the relevant information for the determination. Bottom: ^{1}H NMR spectrum.

In Figure 29 is confirmed what already seen in Figures 14 and 16 for the compound **1**, i.e. the proximity between H-8 (formyl group), H-4 and H-2.

In conclusion:

- the obtained information from the first NOE is that the methyl group is on the same side of H-3 and far from the aromatic ring;
- from the saturation of H-2 is shown that it's on the same side of H-8 (formyl group), H-4 and the aromatic ring. To confirm this, H-3 results on the same side of H-6, as shown in Figure 26.

Therefore, the derived relative configuration for the compound **epi-1** (assuming be *R** the configuration of the quaternary carbon) is 1*R**,2*S**,3*R**,4*R**, hence the epimer at C4 of the major diastereoisomers **1**.

Conformational analysis

The exploration of the PES and subsequent optimization by DFT at the PCM-B3LYP/6-31G(d) level of theory suggested in this case the existence of five conformations comprised into a 2 kcal/mol energy window (Figure 30 and Table 2).

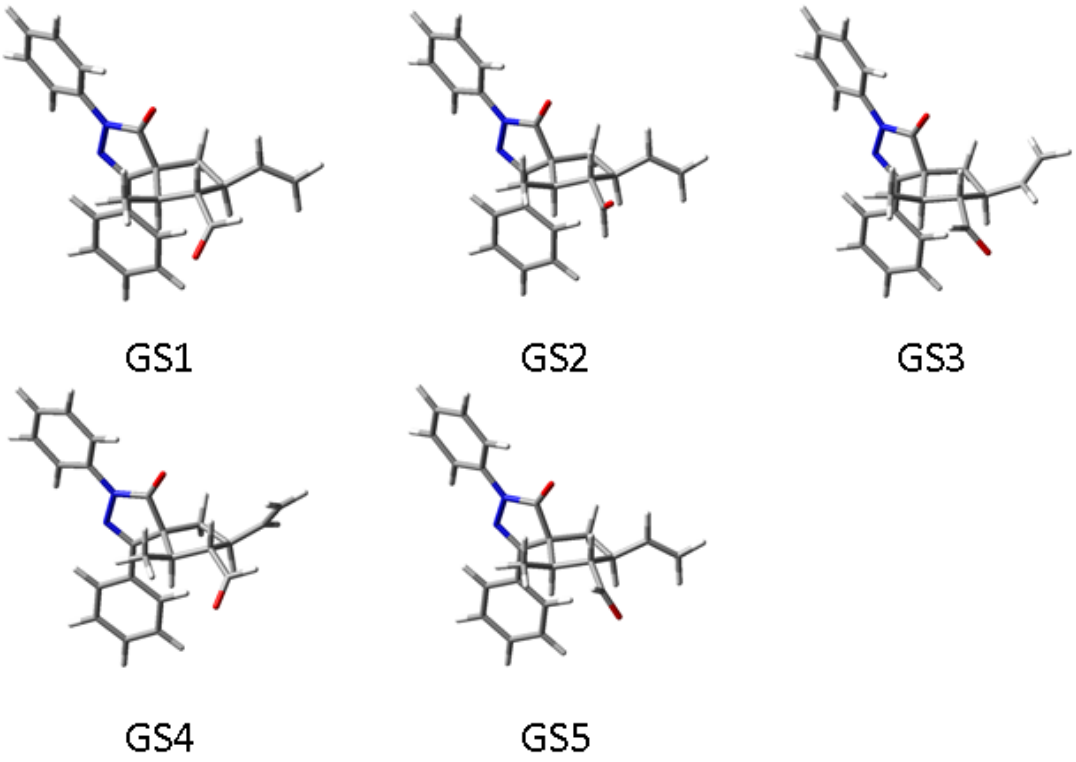

Figure 30 - Optimized structures at the PCM-B3LYP/6-31G(d) level of theory of the 5 best conformations of **epi-1.**

Table 2

Conf.	PCM (acetonitrile)		
	E	H°	Pop(H)
GS1	**0.00**	**0.00**	53
GS2	0.31	0.26	34
GS3	2.01	2.15	1
GS4	1.95	2.01	2
GS5	0.89	0.94	10

Absolute configuration

As in the case of the major diastereoisomer **1**, the absolute configuration was derived from the simulation of the ECD spectrum. The ECD spectrum of **epi-1** (figure 30) shows the same trend of the major diastereoisomer **1**, but with different intensity of the Cotton effects.

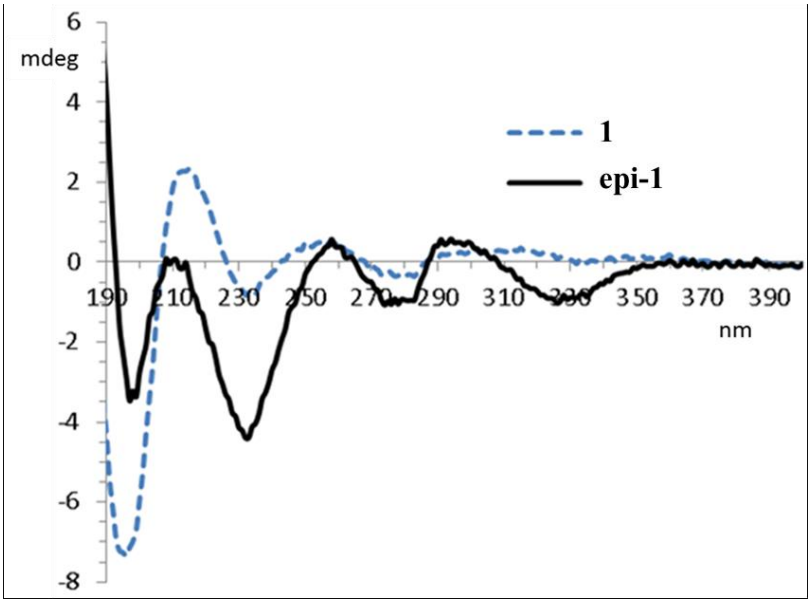

Figure 31 – Experimental ECD spectrum of **1** (black trace) compared with the one of **epi-1** (dotted blue trace).

The simulations of the ECD spectrum were obtained assuming the 1*R*,2*S*,3*R*,4*R* absolute configuration, using the same functionals and basis sets already employed for the major diastereoisomer **1** (Figure 32).

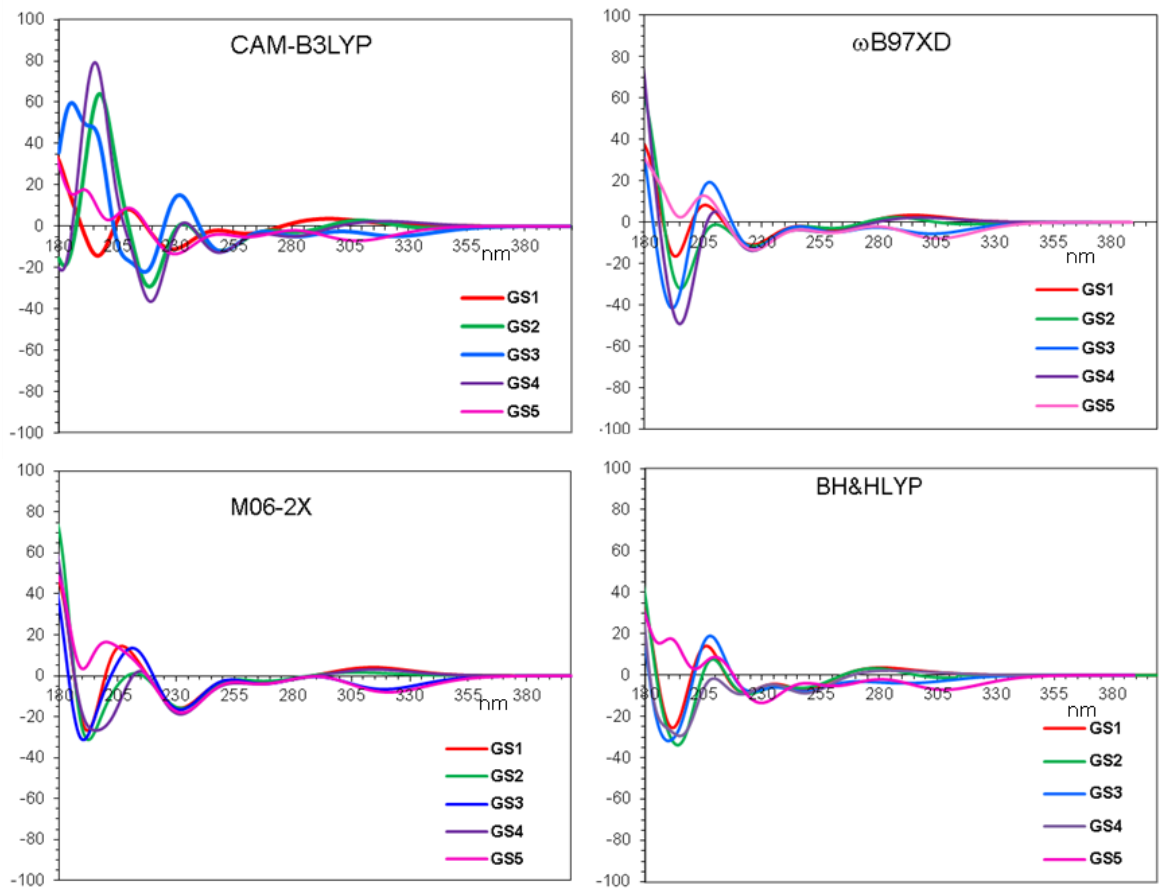

Figure 32 - TD-DFT simulated spectra calculated for the four conformations of **epi-1** using CAM-B3LYP, BH&HLYP, M06-2X, ωB97XD and the 6-311++G(2d,p) basis set. Solvent acetonitrile was included with the PCM formalism. For each conformation, the first 70 excited states were calculated, and the spectrum was obtained using a 0.25 eV line width at half height.

The simulation of the weighted spectrum was obtained by using the populations obtained from Boltzmann distribution and the energies obtained with the PCM-optimization (Table 2, 53:34:1:2:10 for GS1-GS5, respectively).

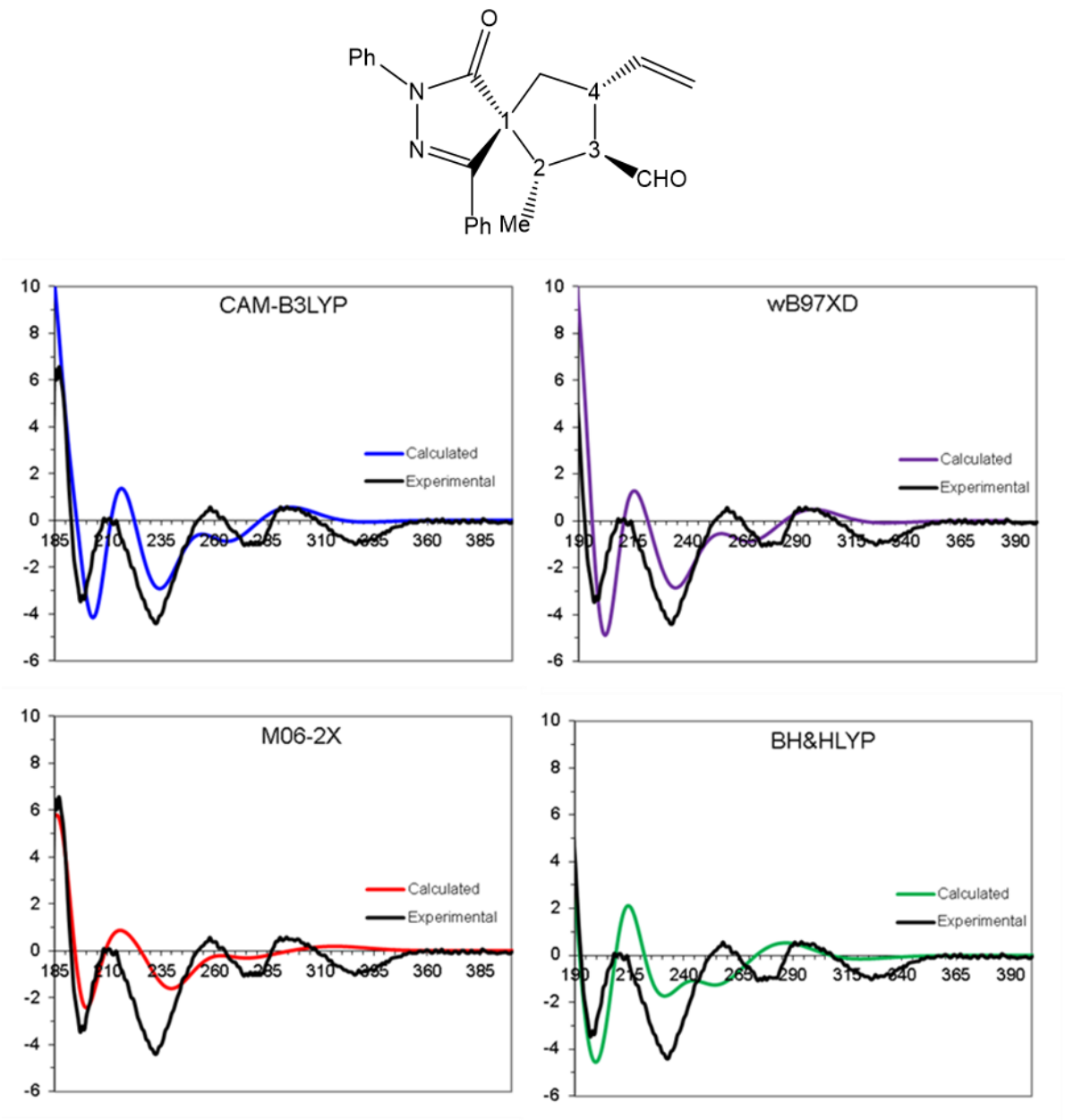

Figure 33 – Simulations of the experimental ECD spectrum of **epi-1**. For each quadrant, the black line corresponds to the experimental spectrum. The colored lines correspond to the simulations obtained using the populations derived from B3LYP/6-31+G(d,p) optimization. All the simulations are for the 1*R*, 2*S*, 3*R*, 4*R* absolute configuration.

The simulations for 1*R*,2*S*,3*R*,4*R* absolute configuration (Figure 33) show a good agreement with the experimental spectrum, particularly when using the CAM-B3LYP and ωB97XD functionals, therefore the absolute configuration identified is 1*R*,2*S*,3*R*,4*R*.

3.3 Results for compound 2

The assignment of the chemical shift of the aliphatic protons was made starting from the hydrogen H-2 at 4.01 ppm, because it is easily identifiable as the only one that generate a doublet. From this signal and by means of the 2D-COSY experiment it has continued with the assignment of H-3 (4.20 ppm), of H-4 (3.94 ppm) and of H-6 (5.96 ppm). The two diastereotopic hydrogens H-5a and H-5b were assigned using the information gained from the NOE spectrum obtained from the saturation of H-4. In this spectrum is showed the spatial proximity between H-4 and the diastereotopic hydrogen that generate the signal at 2.35 ppm, that is the one in a *syn* relationship with H-4 (H-5b). Consequently, the signal of H-5a is the one at 2.09 ppm. The assignment of H-7_E and H-7_Z was made in the same way of the previous cases, so on the basis of the characteristic coupling constant of vinyl hydrogens. Therefore, the signal at 5.16 ppm was attribute at H-7_E while the one at 5.28 ppm at H-7_Z. The assignment of the protons of the aliphatic region was completed by the signals of the methyl groups of the molecule (H-15 and H-20). From the NOE-NMR experiment obtained from the saturation of H-2 it was detected the spatial proximity between H-2 and the methylic hydrogens that generate the signal at 2.27 ppm, which has to be H-15. Consequently, the signal of the methyl hydrogens H-20 is the one at 2.19 ppm.

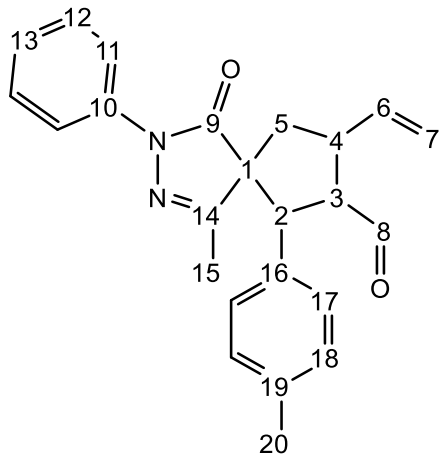

Figure 34 - Compound **2** is shown with carbon number and without proton to clarify.

The assignment of the aromatic region was made starting from the aromatic *ortho*-signal at 7.12 ppm, that is present in the NOE spectrum obtained from the saturation of the H-2 signal, and which it is undoubtedly that of H-17 (due to the excessive distance of H-2 from H-11). By means of the 2D-COSY experiment it was possible to identify H-18 at 7.02 ppm from the correlation with H-17.

By exclusion, the other *ortho*-signal present in the aromatic region of the spectrum must be the one of H-11, found at 7.58 ppm. Then, from COSY correlation with H-11 it was determined the signal of H-12 at 7.32 ppm and consequently that of H-13 at 7.12 ppm.

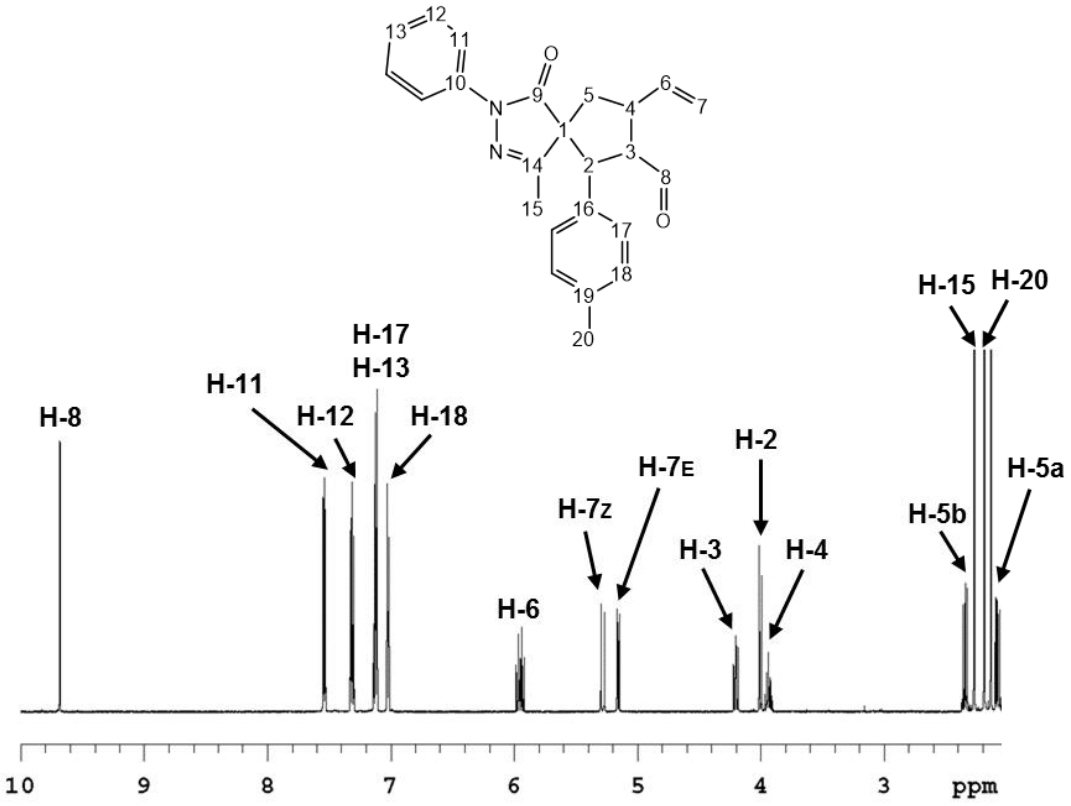

Figure 35 - ^{1}H-NMR spectrum of compound **2** with the full assignment of the hydrogens chemical shifts**.** Signals not indicated are those of the solvent (CD_3CN). The signals of H-17 and H-13 are superimposed.

Relative configuration

The relative configuration of compound **2** was obtained by the analysis of the NOE spectra, as already seen in the previous cases.

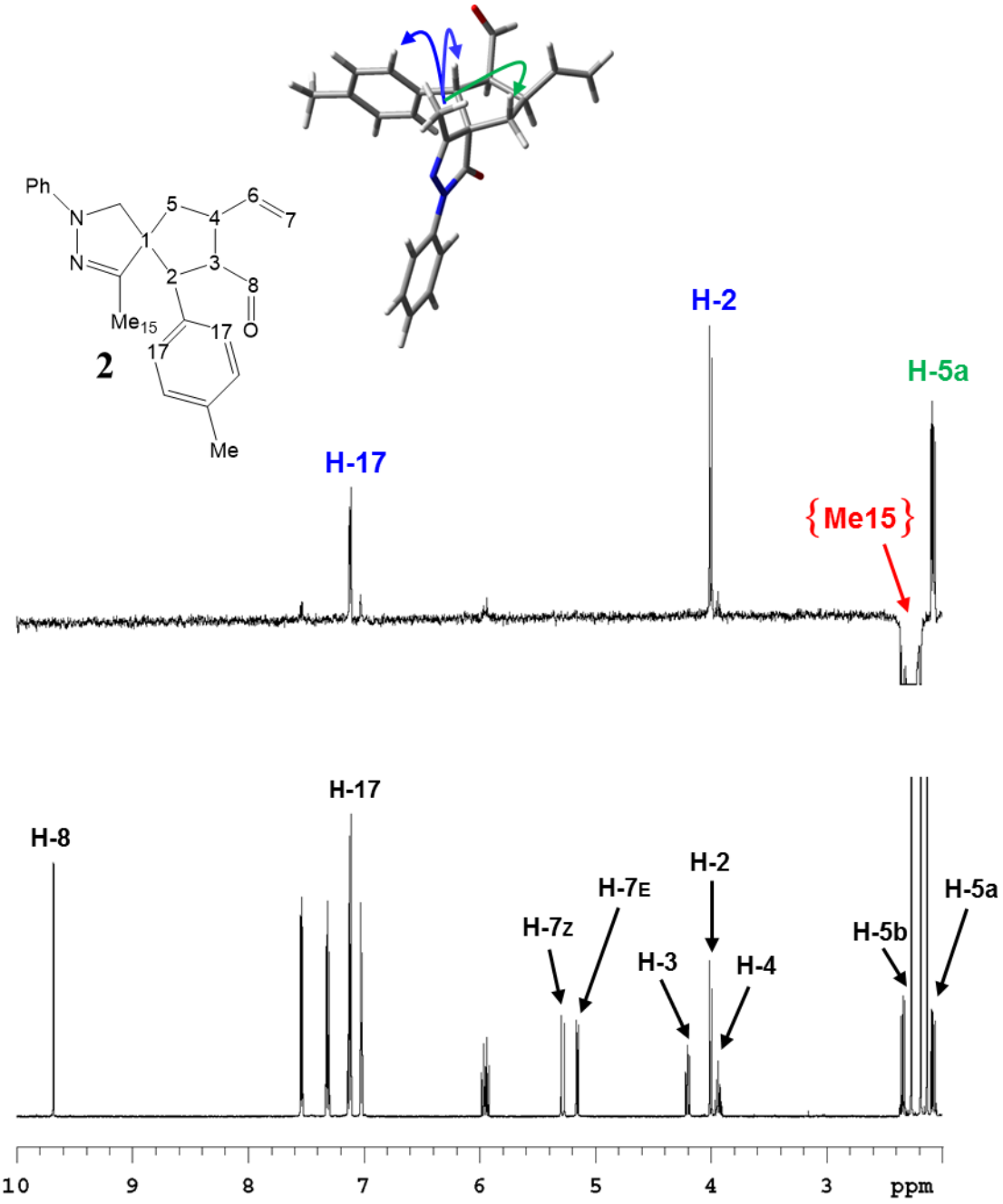

Figure 36 – Top: NOE spectrum obtained from the saturation of the Me-15 hydrogens. In green are shown the "control" signals while the blue ones report the relevant information for the determination. Bottom: ^{1}H NMR spectrum.

By the saturation of the methyl group of the pyrazolone ring, showed in Figure 36 as Me-15, strong NOE is observed with the hydrogen H-2, as well as a not negligible NOE effect with the aromatic hydrogen H-17.

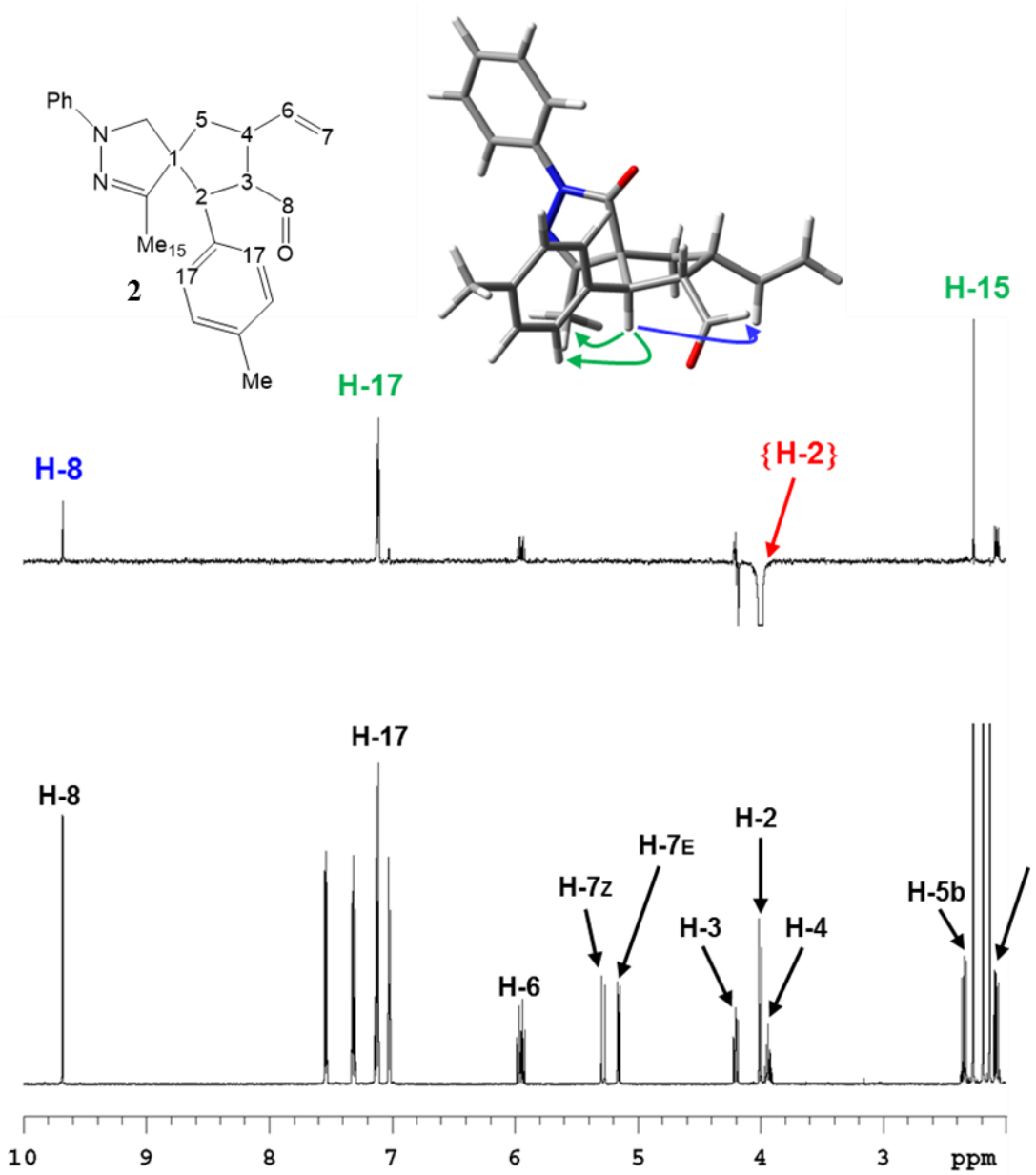

Figure 37 – Top: NOE spectrum obtained from the saturation of H-2. In green are shown the "control" signals while the blue one reports the relevant information for the determination. Bottom: ^{1}H NMR spectrum.

From the saturation of H-2, showed in Figure 37, a small NOE effect is observed with H-8. This information is important for the structural determination, because is showed the proximity between H-2 and H-8. The NOE effect with H-17 and Me-15 are the control signals, not relevant for structural determination.

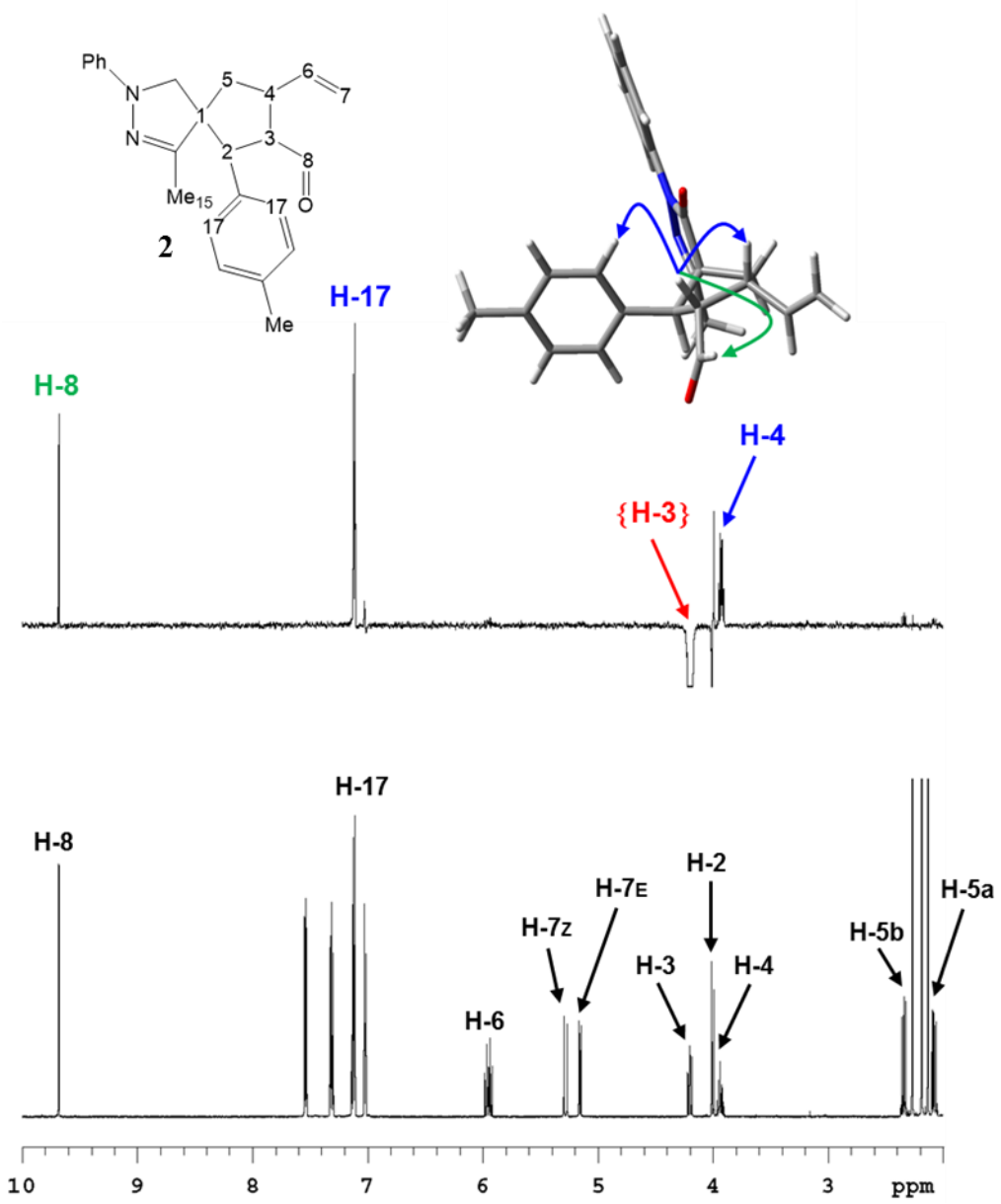

Figure 38 – Top: NOE spectrum obtained from the saturation of H-3. In green are shown the "control" signals while the blue ones report the relevant information for the determination. Bottom: ^{1}H NMR spectrum.

In Figure 38 is showed the NOE spectra obtained when H-3 was saturated. From the latter, two informations were obtained: the proximity between H-3 and H-4 and between H-3 and H-8, but the latter is only a control NOE.

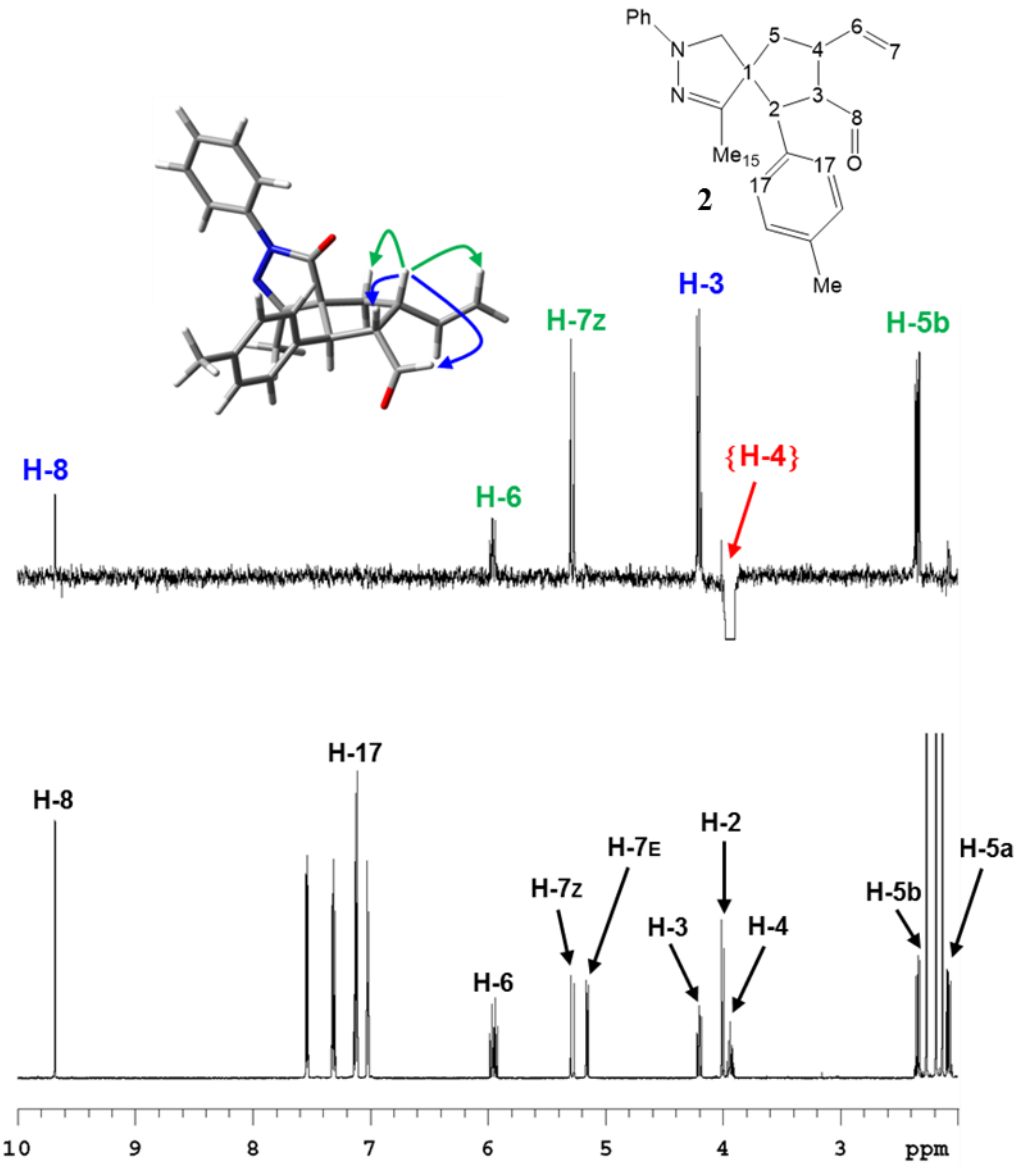

Figure 39 – Top: NOE spectrum obtained from the saturation of H-4. In green are shown the "control" signals while the blue ones report the relevant information for the determination. Bottom: ^{1}H NMR spectrum.

Saturation of H-4 shows large NOE enhancements with H-3 and only small NOE enhancements with H-8. This means that H-4 and H-3 are on the same side of the ring. The NOE effect with H-8 gives information about the preferred conformation of the formyl group.

Further NOE spectra were acquired to gain more redundancy and more information about the preferred conformation.

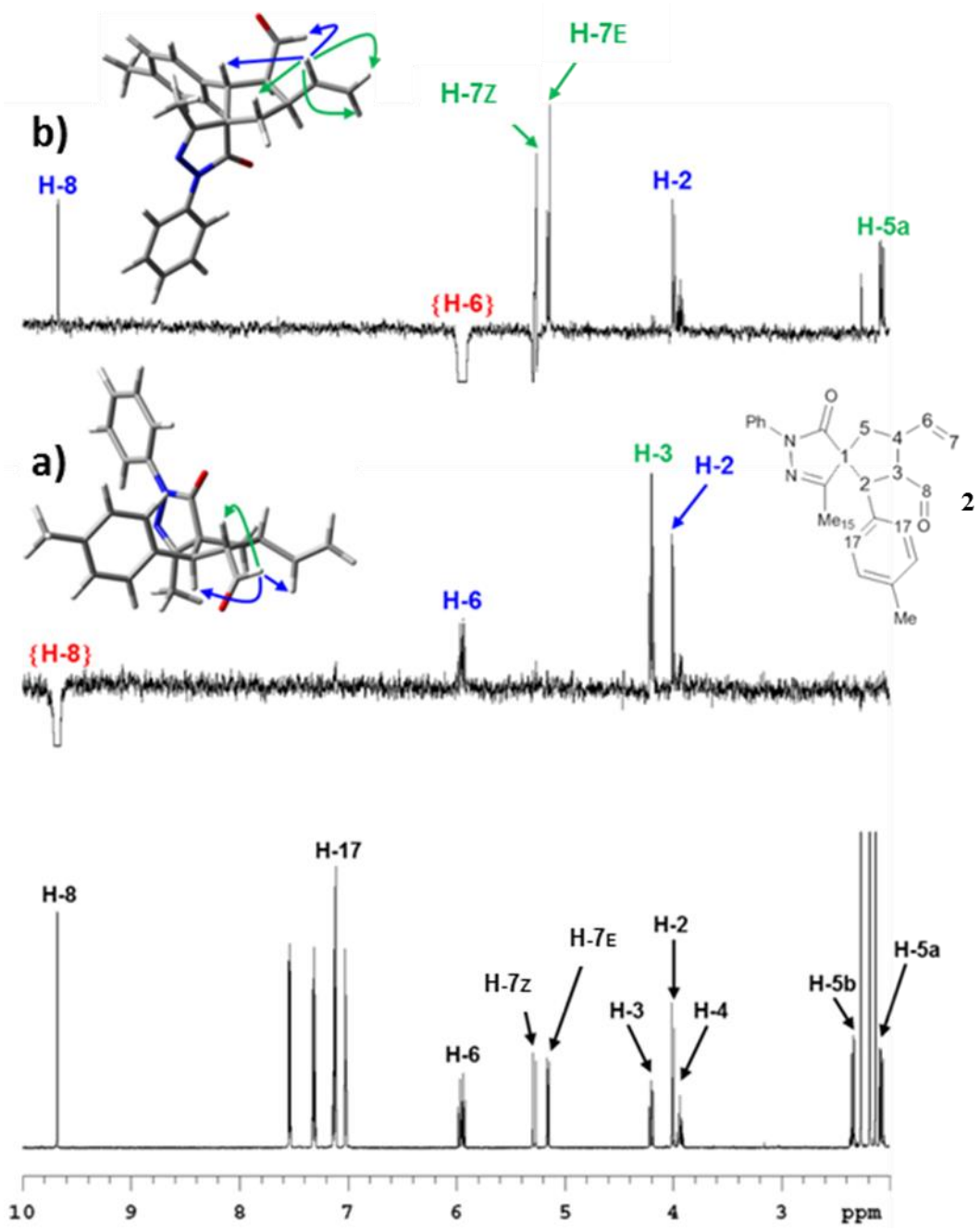

Figure 40 – Top: NOE spectra obtained from the saturation of H-6 (**trace b**) and H-8 (**trace a**). In green are shown the "control" signals while the blue ones report the relevant information for the determination. Bottom: ^{1}H NMR spectrum.

From the saturation of the hydrogen H-8 (**trace a**, Figure 40) it was confirmed what already seen in Figure 35, i.e. the proximity between H-2 and H-8. A NOE effect was observed also with the proton H-6 of the vinyl group. This information confirmed what seen in figures 36 and 37, i.e. the proximity between H-3 and H-4, and consequently that of the formyl group with the vinyl group. The latter is confirmed when H-6 was saturated

(**trace b**, Figure 40). Another NOE effect is seen with H-7_E e H-7_Z are control NOEs.

In conclusion, from the information obtained from the above mentioned spectra it was possible to attribute the relative configuration of the compound **2**.

On saturation of the Methyl signal of pyrazolone (Figure 36) a strong NOE was observed on H-2, but a noticeable NOE was observed also on the *ortho* hydrogens of the phenyl in position 2 (H-17). The spatial proximity between the Methyl and H-2 was confirmed by the saturation of H-2 (Figure 37). In the same spectrum, an intense NOE is visible also on H-6, that implies that the vinyl group is on the same side of H-2 with respect to the cycle. Saturation of H-3 (Figure 38) yields strong NOE on the hydrogen H-17 and on H-4. This means that H-3 and H-4 are on the same side of the cycle and on the opposite side of H-2. The above consideration suggests the 1*R**,2*R**,3*R**,4*S**. It should be noted that the actual spatial disposition of the substituents is the same observed for the major diastereoisomer **1**, and that the different stereochemical descriptor at C2 is due to the higher priority of the phenyl group with respect to the methyl in compounds **1** and **epi-1**.

Conformational analysis

Conformational analysis of **2** yielded again four conformations comprised into a 2 kcal/mol energy window (Table 3). As for **1** and **epi-1**, calculations were run at the B3LYP/6-31G(d) level of theory and including the solvent acetonitrile using the PCM formalism.

Table 3. Calculation at the B3LYP/6-31G(d) level of theory including the solvent with the PCM formalism.

Conf	PCM (acetonitrile)	
	H°	Pop(H)
GS1	**0.00**	69
GS2	0.65	23
GS3	1.44	6
GS4	2.02	2

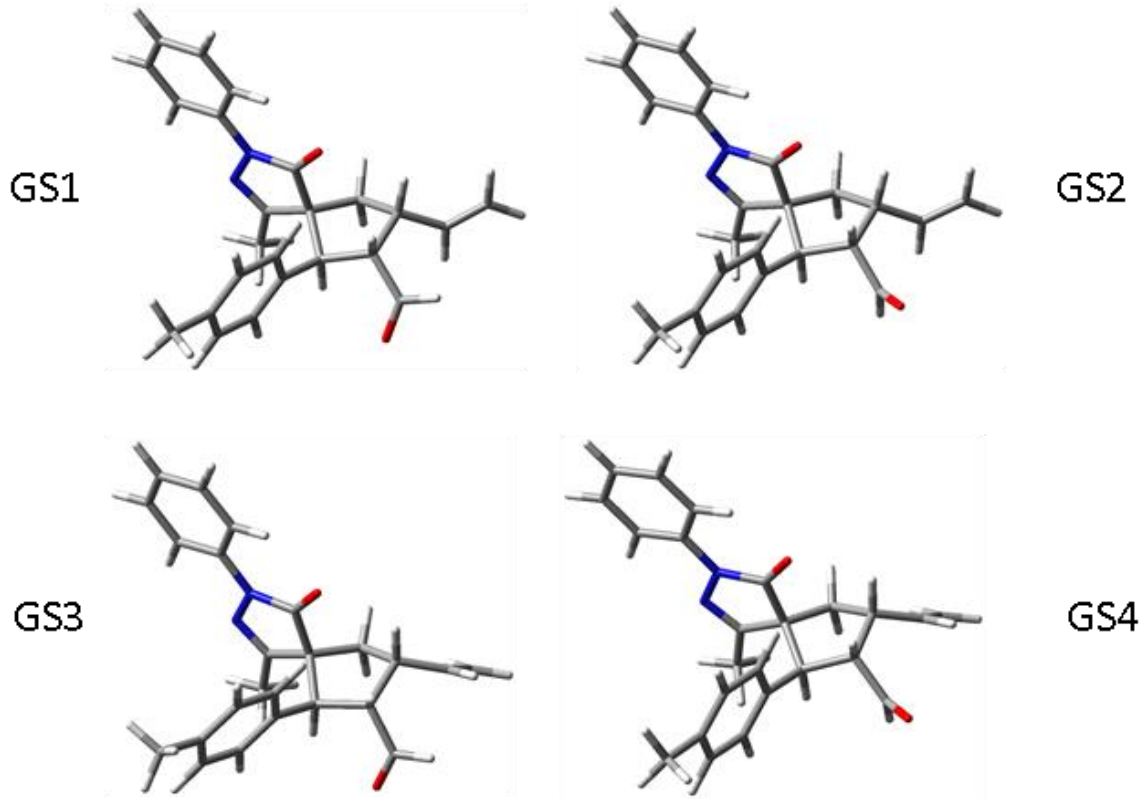

Figure 41 - 3D geometries of the four conformations of **2**

Absolute configuration

The ECD spectrum of **2** was acquired in acetonitrile as in the previous cases. Due to the presence of the phenyl in position 2, tilted out of the plane of pyrazolone, the ECD spectrum is more intense, showing two intense bands at 240 nm and 202 nm (Figure 42). TD-DFT calculation of the ECD spectra of the four conformations were obtained using CAM-B3LYP, BH&HLYP, M06-2X, ωB97XD and the 6-311++G(2d,p) basis set, and the solvent was included using PCM (Figure 43). Compound **2** was obtained with a different catalyst with respect to that used for compound **1**, i.e. a pseudo-enantiomeric catalyst yielding opposite stereocontrol. For this reason the DFT simulations were run supposing the 1*S*,2*S*,3*S*,4*R* absolute configuration.

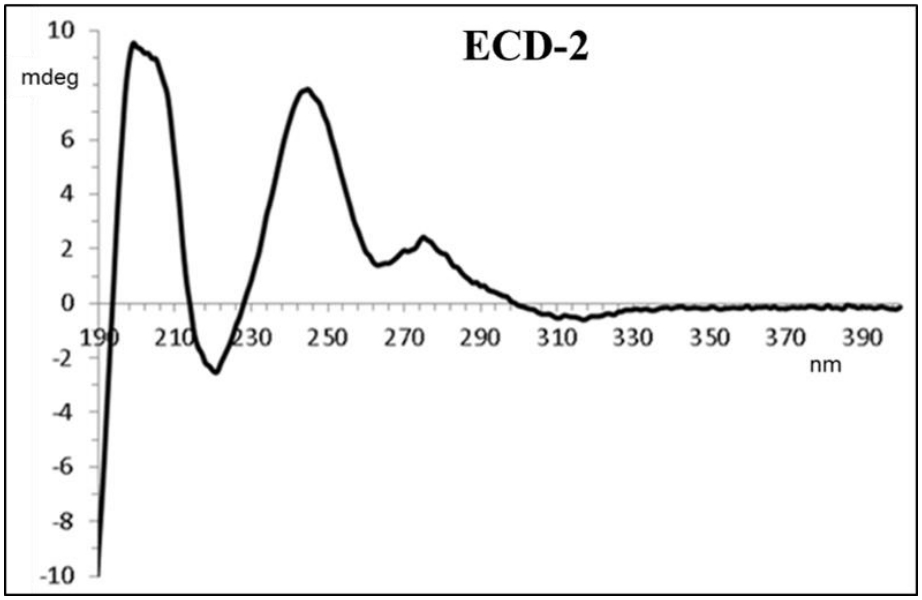

Figure 42 - Experimental ECD spectrum of **2** in acetonitrile

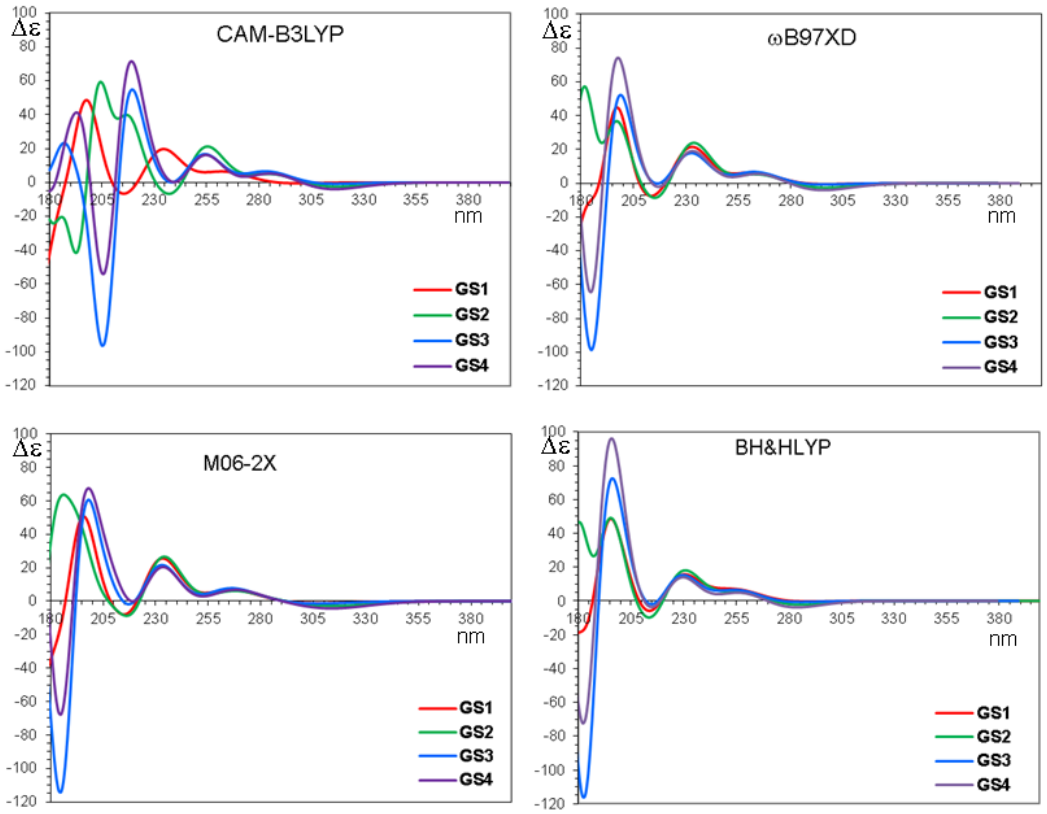

Figure 43 - TD-DFT simulated spectra calculated for the four conformations of compound **2** using CAM-B3LYP, BH&HLYP, M06-2X, ωB97XD and the 6-311++G(2d,p) basis set. Solvent acetonitrile was included with the PCM formalism. For each conformation, the first 70 excited states were calculated, and the spectrum was obtained using a 0.25 eV line width at half height.

The simulation of the experimental ECD spectrum was obtained using the population ratio derived from Boltzmann distribution and the relative energies from Table 3 (69:23:6:2 from GS1-GS4). The simulations for 1*S*,2*S*,3*S*,4*R* absolute configuration (Figure 44) show a good agreement with the experimental spectrum, that is particularly good when using the M06-2X functional, therefore the absolute configuration identified is the 1*S*,2*S*,3*S*,4*R*.

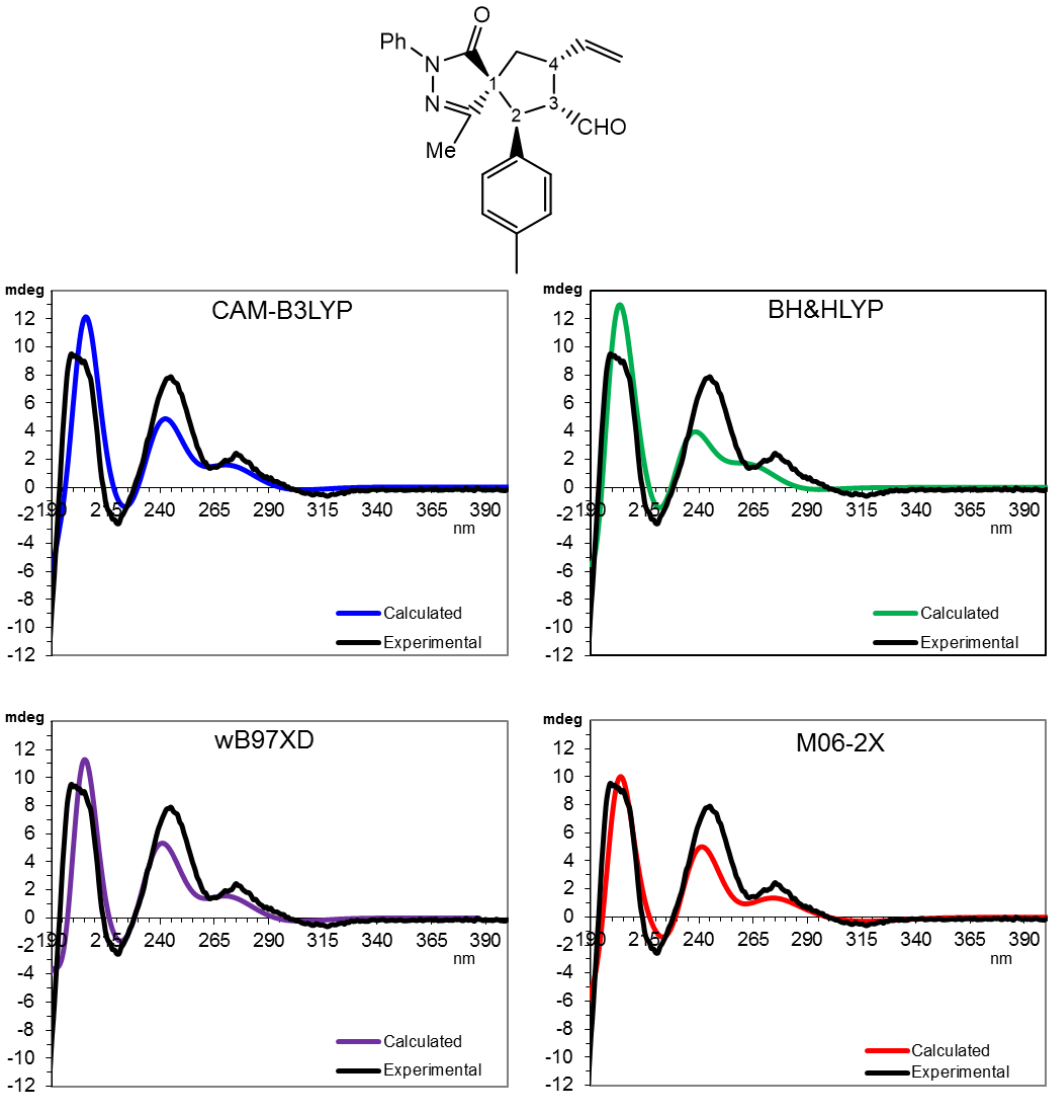

Figure 44 - Simulations of the experimental ECD spectrum of **2**. For each quadrant, the black line correspond to the experimental spectrum. The colored lines correspond to the simulations obtained using the populations derived from B3LYP/6-31+G(d,p) optimization. All the simulations are for the 1*S*,2*S*,3*S*,4*R* absolute configuration.

4 Conclusions

The relative configuration of the four stereocenters of spiropyrazolones **1**, **epi-1** and **2** was determined by NMR-NOE analysis. It turned out that while compound **1** has the *1R*,2S*,3R*,4S** relative configuration, **epi-1** is the diastereoisomer at the C-4 with the *1R*,2S*,3R*,4R** relative configuration.

A full conformational analysis was performed by Molecular Mechanics (MMFF field) scan of the potential energy surface (PES), and the best conformations were optimized by DFT calculations, including the effect of the acetonitrile as solvent in the calculations.

The absolute configuration of the three compounds was then determined by the comparison of the Electronic CD spectra with the simulated spectra obtained by TD-DFT calculations. Four different functionals were used to achieve data redundancy and a more reliable assignment. The 1*R*,2*S*,3*R*,4*S* absolute configuration was determined for **1**, the 1*R*,2*S*,3*R*,4*R* for **epi-1** and the 1*S*, 2*R*, 3*S*, 4*R* for compound **2**. The latter results is in agreement with the chemistry of the reaction, that was performed using the enantiomeric catalyst.

5 Experimental section

5.1 General

Compounds **1**, **epi-1** and **2** were synthesized in Southampton University.

Purification: To separate **1** from **epi-1**, a Phenomenex Luna C18 (5 μm, 100 Å, 250 × 21.2 mm) was used. The mobile phase was a mixture consisting of an azeotrope CH_3CN/H_2O (90%) and H_2O (10%). The flow rate of the mobile phase was 20 mL/min. To purify compound **2**, a C18 column was used (250 x 10 mm) while the eluent was a mixture consisting of 80% of the azeotrope CH_3CN/H_2O and 20% of H_2O. The selected flow rate was, in this case, 5 mL/min.

NMR spectra: NMR spectra were recorded using a spectrometer operating at a field of 14.4 T (600 MHz for ^1H, 150.8 for ^{13}C). Chemical shifts are given in ppm relative to the internal standard tetramethylsilane (^1H and ^{13}C) or relative to the residual peak of the solvents. The assignment of the ^{13}C signals was obtained by means of DEPT, gs-HSQC and gs-HMBC spectra. The 150.8 MHz ^{13}C NMR spectra were acquired under proton decoupling conditions with a 36000 Hz spectral width, 5.5 μs (60° tip angle) pulse width, 1 s acquisition time and 2 s delay time. A line broadening function of 1–2 Hz was applied before the Fourier transformation. NOE spectra were obtained at 600 MHz using the DPFGSE sequence[23] and a 50 Hz wide selective pulse with a R-SNOB shape.[24]

ECD spectra: were recorded with a JACSO J-810 spectropolarimeter at +25 °C in acetonitrile solutions. The concentrations of the samples were tuned to obtain a maximum absorbance of about 1 in the UV spectrum, using a 0.2 cm path length. Spectra were recorded in the 190-400 nm interval, and 16 scans were summed.

Calculations: The conformational searches were preliminarily carried out by means of the Molecular Mechanics Force Field (MMFF), using the Monte Carlo methods.[25] The most stable conformers thus identified were subsequently optimized by DFT computations which were performed by the Gaussian 09 rev D.01 series of programs,[26] using standard optimization parameters. All of the calculations employed the B3LYP hybrid HF-DFT method[27] and the 6-31G(d) basis sets. Frequency calculations proved that the optimized geometries were true ground states (no imaginary frequencies).

ECD simulations: The ECD spectra were simulated by means of TD-DFT calculations. In the calculations, solvent acetonitrile was included with the PCM formalism, and the geometries used for the simulations are that obtained using the populations derived from PCM-B3LYP/6-31G(d) optimization. The calculations were performed using the CAMB3LYP, BH&HLYP, M06-2X and ωB97XD functionals. All the calculations employed the 6-311++G(2d,p) basis set. The simulated spectra were obtained using the first 70 calculated transitions (lowest wavelength about 160 nm) and applying a 0.25 eV line width. The simulated spectra resulting from the Boltzmann averaged sum of the conformations, were vertically scaled and red-shifted to get the best match with the experimental spectrum.

5.2 Spectroscopic data of compounds 1, epi-1 and 2

NMR splitting patterns: singlet (s), doublet (d), triplet (t), quartet (q) and multiplet (m).

Compound 1

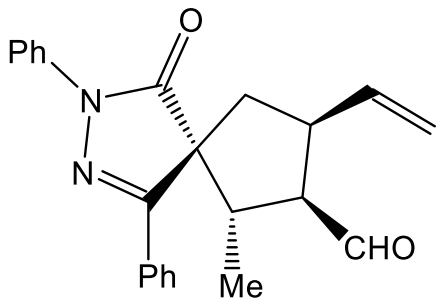

^{1}H NMR (600 MHz, CD_3CN, +25 °C, 1.96 ppm) δ: 0.87 (3H, d, J=6.7), 2.33 (1H, dd, J=13.9, 8.4 Hz), 2.43 (1H, dd, J=13.9, 8.0 Hz), 3.18 (1H, dq, J=10.3, 6.7 Hz), 3.46 (1H, ddd, J= 10.4, 10.3, 1.9 Hz), 3.92 (1H, m, J= 10.4, 9.8, 8.0 Hz), 5.12 (1H, ddd, J= 10.2, 1.6, 0.6 Hz), 5.23 (1H, ddd, J= 16.9, 1.6, 1.0 Hz), 5.88 (1H, ddd, J=16.9, 9.8, 10.2 Hz), 7.26 (1H, m,), 7.47 (2H, m), 7.53 (3H, m, two overlapped signals), 7.92 (2H, m), 7.97 (2H, m), 9.73 (1H, d, J=1.9 Hz);

^{13}C NMR (150.8 MHz, CD_3CN, +25 °C, 118.7 ppm) δ: 13.1 (CH_3), 39.3 (CH_2), 41.6 (CH), 43.4 (CH), 58.6 (CH), 64.1 (Cq), 116.7 (CH_2), 119.4 (CH), 125.6 (CH), 127.3 (CH), 129.3 (CH), 129.4 (CH), 130.8 (two overlapped signals: Cq, CH), 138.4 (Cq), 138.7 (CH), 159.0 (Cq), 175.9 (CO), 203.5 (CHO).

Compound epi-1

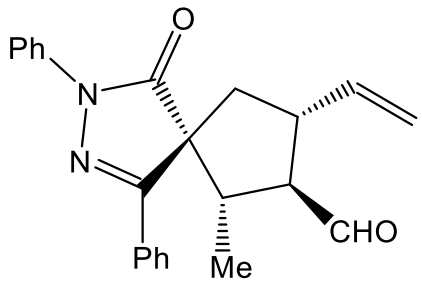

^{1}H NMR (600 MHz, CD_3CN, +25 °C, 1.96 ppm) δ: 0.87 (3H, d, J=6.7 Hz), 2.17 (1H, dd, J=14.7, 9.2 Hz), 2.80 (1H, dd, J=14.7, 9.7 Hz), 2.96 (1H, dq, J= 11.6, 6.7 Hz), 3.06 (1H, ddd, J=11.6, 11.1 3.3 Hz), 3.44 (1H, m, J=11.1, 9.7, 9.2, 8.0, 1.5, 1.01 Hz), 5.12 (1H, ddd, J=10.3, 1.5, 0.7 Hz), 5.22 (1H, ddd, J=17.1, 1.5, 1.01 Hz), 5.98 (1H, ddd, J=17.4, 10.4, 8.0 Hz), 7.26 (1H, m), 7.48 (2H, m), 7.55 (3H, m), 7.98 (4H, m), 9.65 (1H, d, J=3.3 Hz);

^{13}C NMR (150.8 MHz, CD_3CN, +25 °C, 118.7 ppm) δ: 12.0 (CH_3), 39.1 (CH_2), 45.4 (CH), 45.6 (CH), 61.6 (CH), 62.6 (Cq), 117.0 (CH_2), 120.4 (CH), 126.7 (CH), 127.9 (CH), 130.1 (Cq), 130.3 (CH), 130.5 (CH), 131.9 (CH), 139.4 (Cq), 140.6 (CH), 160.4 (Cq), 177.9 (CO), 203.3 (CHO)

Compound 2

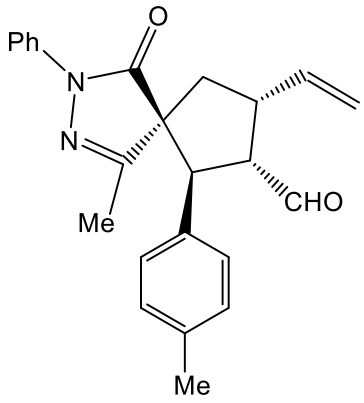

^{1}H NMR (600 MHz, CD_3CN, 25°C, 1.96 ppm) δ: 2.08 (1H, dd, J=13.8, 7.7 Hz), 2.19 (3H , s), 2.27 (3H, s), 2.35 (1H, dd, J= 13.8, 7.9 Hz), 3.93 (1H, m, J= 10.4, 9.5, 7.7, 7.9, 1.0, 0.6 Hz), 4.01 (1H, d, J=11.5 Hz), 4.20 (1H, ddd, J=11.5, 10.4, 2.0 Hz), 5.16 (1H ,ddd , J=10.1, 1.53, 0.6 Hz), 5.28 (1H, ddd, J= 16.9, 1.5, 1.0 Hz), 5.95 (1H, m, J=11.9, 10.1, 9.5 Hz), 7.02 (2H , m), 7.10-7.15 (3H, m), 7.31 (2H ,m), 7.54 (2H, m) 9.68 (1H, d, J=2.0 Hz)

^{13}C NMR (150.8 MHz, CD_3CN, +25 °C, 118.7 ppm) δ: 13.1 (CH_3), 20.4 (CH_3), 38.2 (CH_2), 43.1 (CH), 50.7 (CH), 56.6 (CH), 65.1 (Cq), 116.8 (CH_2), 119.0 (CH), 125.2 (CH), 128.1 (CH), 129.1 (CH), 129.2 (CH), 133.0 (Cq), 137.8 (Cq), 138.2 (Cq), 138.6 (CH), 161.6 (Cq), 175.3 (CO), 202.8 (CHO)

6 Appendix

6.1 Nuclear Overhauser Effect (NOE)

A very important tool in structural and conformational assignment is the proton-proton intramolecular NOE,[28,29,30] that allows to determine which hydrogens are reciprocally close within the molecule. For this reason, the technique is used to elucidate the structures of organic compounds.

The theoretical basis for the NOE was described and experimentally verified by Anderson and Freeman in 1962,[31] following the work of an American physicist, Albert Overhauser, who in 1953 proposed that nuclear spin polarization could be enhanced by the microwave irradiation of the conduction electrons in certain metals. The general Overhauser effect was instead demonstrated experimentally by T. R. Carver and C. P. Slichter, also in 1953,[32] but the theoretical basis and the applicable Solomon equations had already been published by Ionel Solomon in 1955. [6]

The Nuclear Overhauser Effect (NOE) is the transfer of nuclear spin polarization from one spin to another spin *via* cross-relaxation. In other words, NOE effect can be defined as the change in signal intensity of a proton when the equilibrium spin population of another neighbour proton is perturbated by a radiofrequency irradiation. A proton that is close in space to the irradiated one, is affected by the NOE effect independently from the fact that it is scalarly coupled or not with it.

Because of the saturation due to irradiation, a variation of the equilibrium spin population of the neighbour proton is generated. In particular, the irradiation with the radiofrequency generates an increase in the population of the higher energy level of the proton near in space. This excess of population undergoes a relaxation to a lower energy level, predominantly by a dipole-dipole relaxation mechanism and the predominance of intramolecular interactions over intermolecular effects. [33]

Named "S" the irradiated proton and "I" that spatially close to it, and considering the equation derived by Solomon and Bloembergen,[34,35] NOE can be quantitatively described by the following equation: [36]

$$\eta_I\{S\} = \frac{\gamma S}{\gamma I}\left[\frac{\sigma IS}{\rho IS}\right]$$

where:

γ_S and γ_I are the gyromagnetic ratios of S and I, respectively

σ_{IS} is the contribute of the cross relaxation in the total rate

ρ_{IS} is the total relaxation rate

The enhancement of the signal intensity turns out to be proportional to the inverse sixth power of the internuclear distance between the two protons. The maximum positive homonuclear NOE we can ever obtain is 50%, but generally the enhancement of the signal intensity is lower than 20%. Combined together, these two data imply that the measurable effect between ^{1}H-nuclei usually has a distance limit of about 4 Å (0.4 nm).

When performing a NOE experiment, a rather important distinction has to be made between rigid and flexible molecules, because NOE studies of highly flexible molecules are less reliable.[37] When a small and flexible molecule exist in a dynamic equilibrium involving many populated conformers, the observed NOEs is the result of the weighted average of the NOEs of each conformation. In this cases, the only way to get a reliable assignment is to experimentally determine the conformational ratio and the geometry of any populated conformation. This can be done by low temperature NOE-NMR when the interconversion energy barrier is sufficiently high (more than 13-14 kcal/mol).

The NOE-NMR can be used for many applications, and for this reason has become a highly successful technique. In the past years, the use of NOE-NMR in conformational analysis has gained more success because of the high sensitivity and reliability provided by the DPFGSE sequence[23].

6.2 DFT Calculations

Density Functional Theory is a computational technique used to predict the properties of molecules and bulk materials. It is a method for investigating the electronic structure of many-body systems and is based on a determination of a given system's electron density rather than its wavefunction.

Using this theory, the properties of a many-electron system can be determined by using functional, i.e. functions of another function, which in this case is the spatially dependent electron density.

The Density Functional Theory was introduced in the 60's by Hohenberg and Khon, with the two Hohenberg-Kohn theorems.[38]

The first theorem asserts that the ground state properties of a many-electron system depends only on the electronic density, that depends on the three spatial coordinates (x,y,z).

In the second Hohemberg-Khon theorem is proved that the correct ground state density for a system is the one that minimizes the total energy through the functional.
So, if we know the electron density functional, we know the total energy of our system.

One year later, Kohn and Sham reformulated the problem in a more familiar form and opened the way to practical applications of DFT. The system of interacting electrons is mapped on to an auxiliary system of non-interacting electrons moving in an effective potential, having the same ground state charge density. For a system of non-interacting electrons, the ground-state charge density is representable as a sum over one-electron orbitals (the Kohn-Sham orbitals).

The abovementioned effective potential includes the external potential, the effects of the Coulomb interactions between the electrons and the exchange and correlation interactions. Between these terms, the exchange-correlation term remains unknow and must be approximated.

Another approach, less popular than KS-DFT but arguably more closely related to the spirit of the original H-K theorems, is orbital-free density functional theory (OFDFT), in which approximate functionals are also used for the kinetic energy of the non-interacting system.

Like in the case of HF methods, the KS-DFT is an iterative method, but in KS-DFT the electronic correlation is included while in the HF methods the electronic correlation has to be included later.

Due to its favourable cost to performance ratio, DFT is one of the most popular methods available in computational chemistry, for the conformational analysis of organic molecules or to predict the correct geometry and energy of a transition state.

The Time Dependent Density Functional Theory (TD-DFT)[39] is an extension of the DFT method. It is a quantum mechanical theory used in physics and chemistry to investigate the properties and dynamics of many-body systems in the presence of time-dependent potentials, such as electric or magnetic fields. The effect of such fields on molecules and solids can be studied with TD-DFT to extract features like excitation energies, frequency-dependent response properties, and absorption spectra (for example in the simulation of UV and ECD spectra of organic compounds).

DFT in conformational analysis

Density functional theory calculations are very useful for the conformational analysis of organic molecules. They can be applied to calculate the conformation of the ground states, where they proved to be very accurate in the description of geometries and bond lengths when compared with X-ray data.[40] Furthermore, DFT calculations can also be used to find the correct geometry for a transition state.

The application of DFT calculation to conformation analysis is even more challenging than that in a chemical reaction, because in the determination of the energy of conformers is required a good accuracy. For example, if the calculate energy has an uncertainty of ±0.5 kcal/mol this results in an uncertainty of 85% in the relative population of the conformers. From this point of view, DFT confirmed in recent years to be highly reliable in the calculation of the correct energy difference among molecular conformations. However, it should be noted that, as in the case of chemical reactions, there are some cases where the DFT calculations of molecular conformations could not match the experimental evidence. For example, in the case of some aryl-fluorenyl ketones,[41] DFT calculations failed to find the geometry of the best conformation, despite the use of different models and the inclusion of the solvent in the calculations.

As already said before, DFT calculations can also be used to unambiguously find the correct geometry and energy of a transition state, which is a crucial point in conformational analysis, since the correct simulations of energy barriers can greatly help the understanding of dynamic processes detected by dynamic NMR spectroscopy.

Functional and basis sets

One of the most popular functional is the hybrid B3LYP, in which the exchange energy is combined with the exact energy from Hartree-Fock theory. Three parameters define the hybrid functional, specifying how much of the exact exchange is mixed in. The adjustable parameters in hybrid functionals are generally optimized using a 'training set' of molecules, making the DFT methods to lay somewhere between the *ab-initio* method and the semi-empirical ones.

This functional has proved to provide satisfying results in the conformational studies, both in the prediction of the ground state energies and in the prediction of rotational barriers.

However, as determined by recent studies,[42] the failure to take in account dispersion forces in B3LYP functional becomes a big problem when the rotational barriers are particularly high (higher than 30 kcal/mol), i.e. when the transition state is particularly crowded. In this case, the ωB97X-D functional is a valid candidate for the calculation of correct rotational barriers.

In the both *ab-initio* and DFT calculations, the molecular orbitals are calculated as a linear combination of Atomic Orbitals (LCAO); the atomic orbitals are in turn represented as a linear combination of gaussian functions, which are easier to use for the calculation.

The smallest basis set used is generally 6-31G(d): each core orbital is described by a single contraction of 6 GTO (Gaussian Type Orbital) primitives and each valence shell orbital is described by two contractions, one with 3 primitives and the other with 1 primitive; a set of d primitives is added to atoms other than hydrogen.

Interestingly, there is only a small increase in accuracy obtained by using very large basis sets. This is probably due to the fact that the density functional has limited accuracy compared to that of the basis set. The prediction of NMR spectra or ECD spectra, however, requires a more extended basis set, a set of polarization functions is added to

every atom including hydrogen, and diffuse functions are used, i.e. primitives with small exponents, that described the shape of the wave function far from the nucleus. Diffuse functions are important when there are interactions at long distances such as van der Waals interactions. Unfortunately, the use of a larger basis set unavoidably means a large increase of the calculation times.

6.3 Electronic Circular Dichroism (ECD)

The determination of the absolute configuration of chiral molecules is an important aspect of molecular stereochemistry. Although the most reliable method is the anomalous dispersion X-ray crystallography, in recent years an increasing number of papers describing the AC assignment by chiroptical methods have been presented, because these methods can manage any compound that cannot be crystallized. On the other hand, the theoretical simulations have shown to be highly reliable when dealing with rigid molecules, the main weakness of any chiroptical technique being the conformational freedom of many organic molecules., and the risk to overlook a populated conformation. For this reason, before calculating any optical property, an accurate conformational analysis must be carried out.

Among the chiroptical techniques, the most widely used to detect and analyse chirality of a molecular system is the determination of the optical activity by circular dichroism[43] (CD).

A CD experiment consist in alternately radiating a chiral sample with equal amount of left and right circularly polarized light of a selected wavelength. The circularly polarized light itself is chiral and interact differently with chiral molecules. That means that, depending on the chromophore groups of the molecule, at certain wavelengths the two types of circularly polarized light are absorbed to different extents.

The result of the analysis is the wavelength-dependent difference of absorption that is defined as the difference between the absorption of the left and the right circularly polarized light.

$$\Delta A = A_L - A_R$$

The difference of absorption can also easily converted in molar circular dichroism, defined as the difference between the molar absorption coefficients of left and right circularly polarized light.

$$\Delta\varepsilon = \varepsilon_L - \varepsilon_R$$

The CD spectrum features the $\Delta\varepsilon$ as a function of the wavelength. The Electronic Circular Dichroism (ECD) is a CD experiment conducted with UV-VIS radiation, so that the electronic transition tale place.

Usually, any electronic transition that gives rise an UV-visible absorption also gives rise to a band in the CD spectrum, called "Cotton effect"; the maximum (or the minimum for bands with negative sign) of the cotton effect is usually at the same wavelengths of the maximum of the UV-visible absorption.

Two enantiomers of a chiral molecule are expected to yield mirror image CD spectra, which differ in sign but not in amplitude. An example is reported in Figure 45.

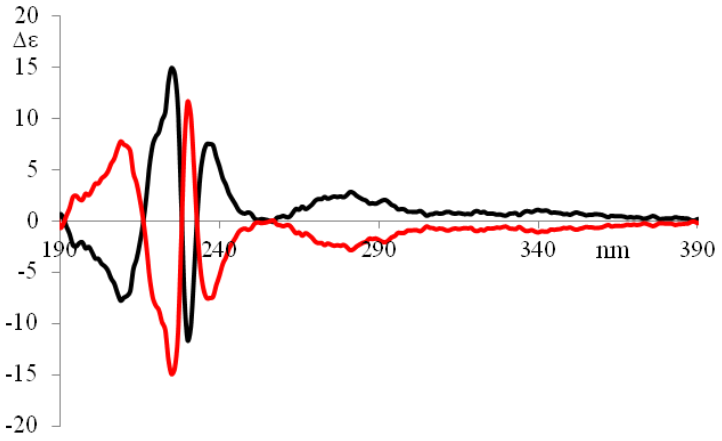

Figure 45 - Experimental ECD spectra of two *anti*-atropoisomers of 3,4-Bisaryl-N-benzylmaleimides[44]

The sign of the CD spectrum does not depend from the absolute configuration of the enantiomer. That because the CD spectra are conditioned by the chromophores in their environment, and depend on details of the electronic and geometric molecular structure.[45] For this reason, the simple comparison of the CD spectra of two similar compounds doesn't necessary lead to the determination of absolute configuration. However, the

sensitivity to the absolute configuration as well as to conformational features, which are often completely obscured in the ordinary absorption spectrum, makes circular dichroism one of the most powerful techniques for stereochemical analysis.[46]

The way to determine the absolute configuration of a molecule by means of the CD spectrum is to compare the experimental spectrum with a calculated theoretical curve, obtained by the appropriate method (DFT or TD-DFT). Time-dependent density functional theory (TD-DFT) is presently the most widely used electronic structure method for ECD calculations. It extends the basic ideas of ground state density-functional theory (DFT) to the treatment of excitations or more general time-dependent phenomena. The use of the solvent in the calculations is very important, since ECD depends sensitively on the presence and nature of solvent interactions.[47] However, the change in chiroptical response due to solute-solvent interactions is sometimes drastic and non-intuitive.

Since the ECD spectra strongly depends on the conformation of the molecule, it is important to calculate the spectra for all of the ground states found in a conformational analysis. A Boltzmann weighting of the simulated spectra for all the conformations allows the comparison with the experimental results. Even with the simplest approximation to the Kohn-Sham potential, spectra calculated within this framework are in very good agreement with experimental results.[48] An example of experimental and calculated comparison is reported in figure.

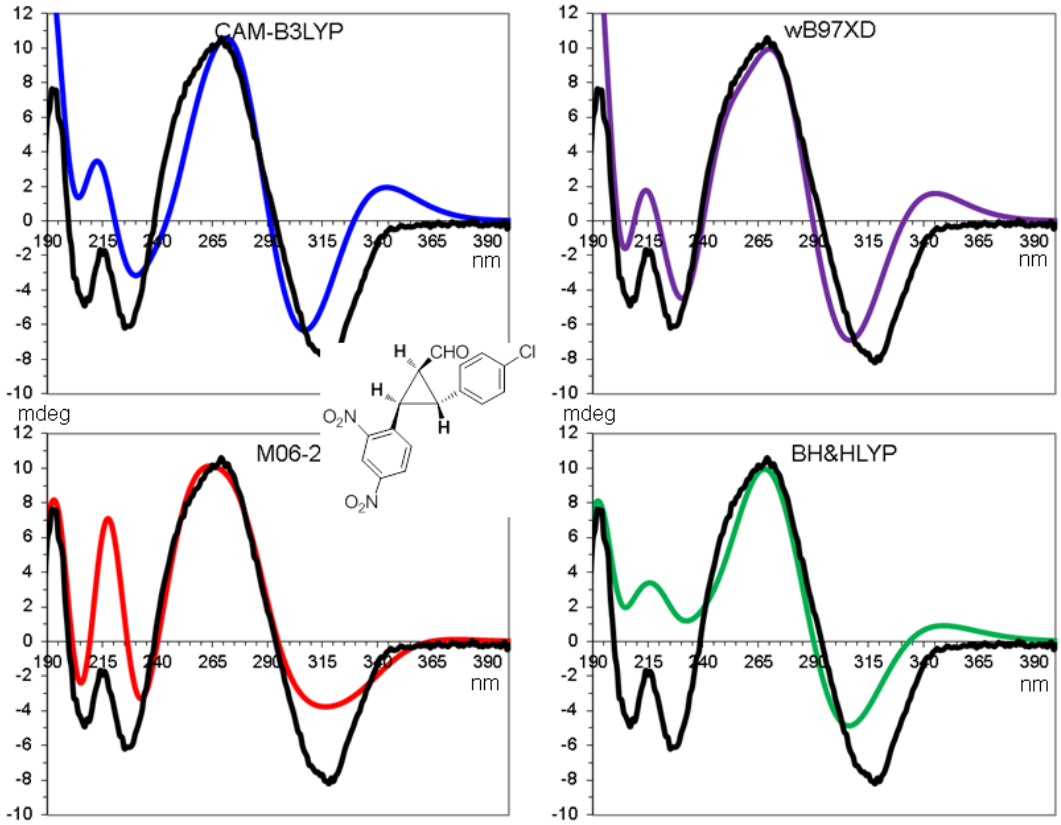

Figure 46 – Example of a comparison of an experimental and calculated ECD spectra [49]

7 Bibliography

[1] Tietze, L. F.; Beifuss, U. *Angew. Chemie Int. Ed.* **1993**, *32*, 131–163.

[2] Robinson, R. *J. Chem. Soc. Trans.* **1917**, *111*, 762

[3] Padwa, A.; Bur, S. K. *Tetrahedron* **2007**, *63*, 5341–5378.

[4] Pellissier, H. *Tetrahedron*, **2006**, **62**, 1619–1665.

[5] Nicolaou, K. C.; Edmonds, D. J.; Bulger, P. G. *Angew. Chemie Int. Ed.* **2006**, *45*, 7134–7186.

[6] Enders, D.; Hüttl, M. R. M.; Grondal, C.; Raabe, G. *Nature*, **2006**, *441*, 861–863.

[7] Hassan, A.E.; Moustafa, A.H.; Tolbah, M.M; HF Zohdy; AZ Haikal. *Nucleosides Nucleotides Nucleic Acids*, **2012**, *31*, 783-800.

[8] Mariappan, G.; Saha, B.P.; Sutharson, L.; Singh, A.; Garg, S.; Pandey, L.; Kumar, D. *Saudi Pharm. J.*, **2011**, *19*, 115- 122.

[9] Saidachary, G.; Veera Prasad, K.; Divya, D.; Singh, A.; Ramesh, U.; Sridhar, B.; China Raju, B. *Eur. J. Med. Chem.*, **2014**, *76*, 460-469.

[10] Wang, X.H.; Wang, X.K.; Liang, Y.J.; Shi, Z.; Zhang, J.Y.; Chen, L.M.; Fu, L.W. *Chin. J. Cancer*, **2010**, *29*, 980-987.

[11] Hadi, V.; Koh, YH; Sanchez, T.W.; Barrios, D.; Neamati, N.; Jung, K.W. *Bioorg. Med. Chem. Lett.*, **2010**, *20*, 6854-6857.

[12] Datar, P.A.; Jadhav, S.R. *Int. J. Med. Chem.*, **2015**, *2015*, 670181.

[13] Wang, W.; Li, H.; Wang, J. *Org. Lett.*, **2005**, *7*(8), 1637–1639

[14] Peerdeman, A.F.; Van Bommel, A.J.; Bijovet, J.M.; *Nature*, **1951**, *168*, 271-271

[15] Hooft, R. W. W.; Straversa, L. H.; Spek, A. L. *J. Appl. Cryst.*, **2008**, *41*, 96-103

[16] For reviews see: a) G. Bringmann, T. Bruhn, K. Maksimenka, Y. Hemberger, *Eur. J. Org. Chem.* **2009**, 2717-2727. b)T. D. Crawford, M. C. Tam, M. L. Abrams, *J. Chem. Phys.*, **2007**, *111*, 12057–12068. c) G. Pescitelli, L. Di Bari, N. Berova, *Chem. Soc. Rev*.

2011, *40*, 4603-4625. For a review on conformational analysis for the absolute configuration determination see: A. Mazzanti, D. Casarini, D. *WIREs Comput. Mol. Sci*. **2012**, *2*, 613-641

[17] In Gaussian 09 the BH&HLYP functional has the form: 0.5*EXHF + 0.5*EXLSDA + 0.5*ΔEXBecke88 + ECLYP

[18]Y. Zhao and D.G. Truhlar, *Theor. Chem. Acc*. **2008**, *120*, 215-241.

[19] J-D. Chai and M. Head-Gordon, *Phys. Chem. Chem. Phys.*, **2008**, *10*, 6615-6620.

[20] T. Yanai, D. Tewand, and N.Handy, *Chem. Phys. Lett.* **2004**, *393*, 51-57.

[21] a) M. Meazza, M. E. Light, A. Mazzanti and R. Rios. *Chem. Sci.* **2016**, *7*, 984; b) P. Gunasekaran, S. Perumal, J. Carlos Menéndez, M. Mancinelli, S. Ranieri, A. Mazzanti, *J. Org. Chem.* **2014**, *79***,** 11039–11050. c) L. Caruana, M. Fochi, M. Comes Franchini, S. Ranieri, A. Mazzanti, L. Bernardi, *Chem. Commun.* **2014**, *50*, 445-447. d) M. Ambrogi, A. Ciogli, M. Mancinelli, S. Ranieri, A. Mazzanti, *J. Org. Chem.* **2013**, *78*, 3709-3719. e) L. Caruana, M. Fochi, S. Ranieri, A. Mazzanti, L. Bernardi, *Chem. Commun.* **2013**, *49*, 880-882.

[22]P.J. Stephens, D.M. McCann, F.J. Devlin, J.R. Cheeseman and M.J. Frisch, *J. Am. Chem. Soc.* **2004**, *126*, 7514-7521

[23] Stonehouse, J.; Adell, P.; Keeler, J.; Shaka, A. J. *J .Am. Chem. Soc.* **1994**, *116*, 6037–6038.

[24] Kupče, E.; Boyd, J.; Campbell, I.D. *J. Magn. Reson. Series B*, **1995**, *106*, 300–303.

[25] MonteCarlo search with the MMFF force field, as implemented in TITAN 1.0.5, Wavefunction, Inc., Irvine, CA.

[26] Gaussian 09, rev D.01: Frisch, M. J.; Trucks, G. W.; Schlegel, H.B.; Scuseria, G. E.; Robb, M. A.; Cheeseman, J. R.; Scalmani, G.; Barone, V.; Mennucci, B.; Petersson, G. A.; Nakatsuji, H.; Caricato, M.; Li, X.; Hratchian, H. P.; Izmaylov, A. F.; Bloino, J.;

Zheng, G.; Sonnenberg, J. L.; Hada, M.; Ehara, M.; Toyota, K.; Fukuda, R.; Hasegawa, J.; Ishida, M.; Nakajima, T.; Honda, Y.; Kitao, O.; Nakai, H.; Vreven, T.; Montgomery, J. A., Jr.; Peralta, J. E.; Ogliaro, F.; Bearpark, M.; Heyd, J. J.; Brothers, E.; Kudin, K. N.; Staroverov, V. N.; Kobayashi, R.; Normand, J.; Raghavachari, K.; Rendell, A.; Burant, J. C.; Iyengar, S. S.; Tomasi, J.; Cossi, M.; Rega, N.; Millam, N. J.; Klene, M.; Knox, J. E.; Cross, J. B.; Bakken, V.; Adamo, C.; Jaramillo, J.; Gomperts, R.; Stratmann, R. E.; Yazyev, O.; Austin, A. J.; Cammi, R.; Pomelli, C.; Ochterski, J. W.; Martin, R. L.; Morokuma, K.; Zakrzewski, V. G.; Voth, G. A.; Salvador, P.; Dannenberg, J. J.; Dapprich, S.; Daniels, A. D.; Farkas, Ö.; Foresman, J. B.; Ortiz, J. V.; Cioslowski, J.; Fox, D. J. Gaussian, Inc., Wallingford, CT, 2009.

[27] (a) Lee, C.; Yang, W.; Parr, R. G. *Phys. Rev. B* **1988**, *37*, 785−789. (b) Becke, A. D. J. *Chem. Phys.* **1993**, *98*, 5648−5652. (c) Stephens, P. J.; Devlin, F .J.; Chabalowski, C. F.; Frisch, M. J. J. *Phys. Chem.* **1994**, *98*, 11623−11627.

[28] Overhauser, A.W.; *Phys. Rev* **1953**, *92*, 411-415.

[29] Noggle, J.H.; Schrimer R.E. *The Nuclear Overhauser Effect. Chemical applications*. New York: Academic Press, **1971**.

[30] Neuhaus, D.; Williamson, M.P.; *The Nuclear Overhauser Effect in Structural and Conformational Analysis*, 2nd edition, New-York: Wiley-VCH, **2000**, 456-484

[31] Anderson, W. A.; Freeman, R. *The Journal of Chemical* Physics, **1962**, *37*, 411–5

[32] Carver, T. R.; Slichter, C. P. *Physical Review*, **1953**, *92*, 212–213.

[33] Mazzanti, A.; Casarini, D. *WIREs Comput. Mol. Sci.* **2012**, *2*, 613-641.

[34] Solomon, I. *Phys. Rev.*, **1955**, *99*, 559-565

[35] Solomon, I.; Bloembergen, N. *J. Chem. Phys.* **1956**, *25*, 261-266

[36] Claridge, T.D.W. *High-Resolution NMR Techniques in Organic Chemistry*, 2nd edition, Amsterdam: Pergamon Press, **2009**, Chapter 8

[37] Casarini, D.; Foresti, E.; Gsparrini, F.; Lunazzi, L.; Macciantelli, D.; Misiti, D.; Villani, C. *J. Org. Chem*., **1993**, *58*, 5674-5682.

[38] Hohenberg, P.; Kohn, W. *Phys. Rev.* **1964**, *136,* B864–B871

[39] Runge, E.; Gross, E. K. U. *Phys. Rev. Lett.* **1984**, *52,* 997–1000.

[40] Petrukina, M.A.; Andreini, K.W.; Mack, J.; Scott, L.T.

[41] Casarini, D.; Lunazzi, L.; Mazzanti, A. *Org. Biomol. Chem.* **2009**, *7*, 1619-1626.

[42] Masson, E. *Org. Biomol. Chem.*, **2013**, *11*, 28549-2871

[43] Berova, N.; Nakanishi, K.; Woody, R. W.; *Circular dichroism, Principles and applications*, 2nd edition, Wiley-VCH, **2000**.

[44] Ambrogi, M.; Ciogli, A.; Mancinelli, M.; Ranieri, S.; Mazzanti, A. *J. Org. Chem.* **2013**, *78*, 3709-3719.

[45] Warnke I., Furche F. *WIREs Comput. Mol. Sci.* **2012**, *2*, 150-166.

[46] Mazzanti, A.; Casarini D.; *WIREs Comput. Mol. Sci.* **2012**, *2*, 613-641.

[47] a) Kongsted, J.; Pedersen, T. B.; Osted A.; Hansen, A. E.; Mikkelsenm K.V.; Christiansen, O. *J. Chem. Phys. A* **2004**, *108*, 3632-3641. b) Müller, T.; Wiberg, K. B.; Vaccaro, P. H. *J. Chem. Phys. A* **2000**, *104*, 5959-5968. c) Kumata, Y.; Furukawa, J.; Fueno, T. *Bull. Chem. Soc. Jpn.* **1970**, *43*, 3920-3921. d) Mukhopadhyay, P.; Zuber, G.; Goldsmith, M.; Wipf, P.; Beratan, D. N. *Chem. Phys. Chem.* **2006**, *7*, 2483-2486.

[48] Marques, M. A. L.; Gross, E. K. U. *Annu. Rev. Phys. Chem.*, **2004**, *55*, 427-55.

[49] Meazza, M.; Light, M.E.; Mazzanti, A.; Rios, R. *Chem. Sci.* **2016**, *7*, 984-988.